Review | Open Access

Energy Materials

Zhang *et al. Energy Mater.* **2026**, *6*, 600066 **DOI:**10.20517/energymater.2026.56

Interfacial engineering of Bi-based heterojunction for boosting photocatalytic nitrogen fixation: a perspective review

Danrui Zhang#, Li Guo#, Zixuan Li, Tianyu Wang*, Chunming Yang*, Danjun Wang*

Keywords:
Photocatalytic ammonia synthesis, bismuth-based materials; heterojunctions, nitrogen fixation, reaction mechanisms

Citation: Zhang, D.; Guo, L.; Li, Z.; Wang, T.; Yang, C.; Wang, D. Interfacial engineering of Bi-based heterojunction for boosting photocatalytic nitrogen fixation: a perspective review. *Energy Mater.* **2026**, *6*, 600066. https://dx.doi.org/10.20517/energymater.2026.56

Received: 7 Apr 2026
First Decision: 30 Apr 2026
Revised: 11 May 2026
Accepted: 28 May 2026
Published: 18 Jun 2026

Academic Editor:
Jiaqi Huang
Copy Editor:
Ping Zhang
Production Editor:
Ping Zhang

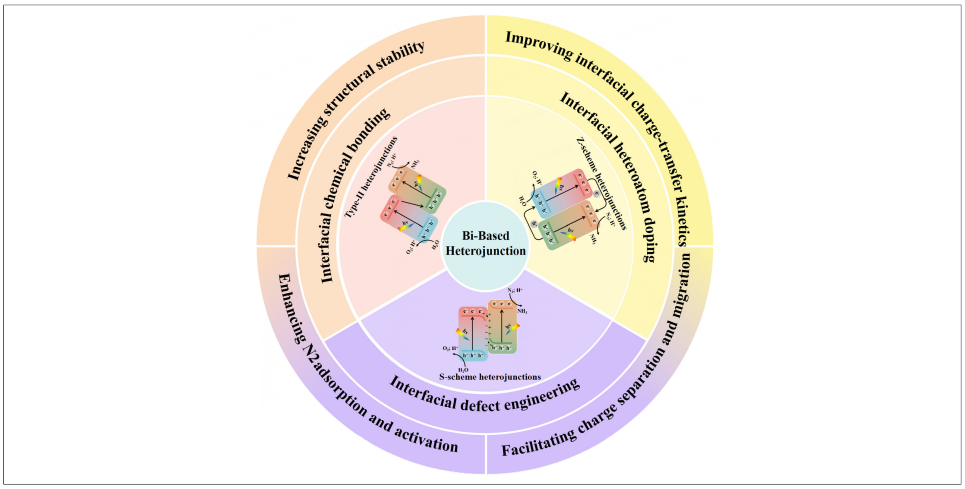

Abstract

Photocatalytic ammonia synthesis, which leverages solar energy to convert nitrogen and water into ammonia, presents a sustainable and environmentally friendly alternative to the energy-intensive Haber-Bosch process. However, the effective activation of the particularly strong N≡N bond remains a significant challenge. Bismuth (Bi)-based materials have been identified as promising photocatalysts due to their strong absorption of visible light, high nitrogen adsorption capacity, and low toxicity. To further improve their photocatalytic performance, extensive research has been directed toward the design of Bi-based heterojunctions. This review highlights the essential and often decisive influence of heterojunction interface engineering in enhancing photocatalytic nitrogen fixation performance. Unlike traditional heterojunction construction, precise interfacial engineering - including the development of built-in electric fields, chemical bonds at the interface, atomic-scale charge transfer pathways, and defect-mediated active sites can fundamentally modulate charge separation, promote N_2 adsorption and activation, and enhance structural stability. A systematic summary of recent advancements in various Bi-based heterojunctions (e.g., Type II, Z-scheme, and S-scheme) is provided, with

Yan'an Key Laboratory of Green Catalysis and Quality Improvement and Utilization of Low Rank Coal, College of Chemistry & Chemical Engineering, Yan'an University, Yan'an 716000, Shannxi, China.
#Authors contributed equally.

*Correspondence to: Prof. Danjun Wang, Prof. Chunming Yang, Dr. Tianyu Wang, Yan'an Key Laboratory of Green Catalysis and Quality Improvement and Utilization of Low Rank Coal, College of Chemistry & Chemical Engineering, Yan'an University, Yan'an 716000, Shannxi, China. E-mail: wangdj761118@yau.edu.cn; chunmingyang@yau.edu.cn; wangty@yau.edu.cn

particular emphasis on how interface design governs reaction mechanisms and catalytic efficiency. Finally, current challenges and future perspectives are discussed to inform the rational design of high-performance catalysts and to further the development of photocatalytic nitrogen fixation through interface-focused strategies.

INTRODUCTION

As an essential precursor to synthetic fertilizers, ammonia (NH_3) serves as a cornerstone of modern intensive agriculture. Its widespread production and application substantially enhance crop yields, thereby playing a critical role in supporting global food security and sustaining a growing population[1-3]. Currently, industrial-scale ammonia production relies almost exclusively on the Haber-Bosch process, which meets global demand but poses significant scientific and environmental challenges[4-6]. The core scientific hurdle lies in the reduction of molecular nitrogen (N_2) to NH_3, a reaction hindered by the exceptionally high dissociation energy of the N≡N triple bond (941 kJ·mol^{-1})[7-9]. To overcome this kinetic and thermodynamic barrier, the Haber-Bosch process employs iron-based catalysts under harsh conditions (400-500 °C, 150-250 bar)[10,11]. Furthermore, its reliance on natural gas as the hydrogen source results in substantial CO_2 emissions, accounting for approximately 1%-2% of global greenhouse gas output. These drawbacks have motivated extensive research into sustainable alternatives that minimize both energy consumption and environmental impact[4].

Photocatalytic nitrogen fixation has emerged as a promising pathway that operates at ambient conditions using solar energy. Unlike the dissociative mechanism of Haber-Bosch synthesis, the photocatalytic system often follows an associative pathway [with an overpotential ~0.4-0.5 V *vs.* Reversible Hydrogen Electrode (RHE) in alkaline media], which enables the stepwise hydrogenation of N_2 without cleaving the N≡N bond prematurely[12,13]. This mechanism preserves the N-N bond until the final reaction stages, thereby significantly decreasing the energy input. Since the pioneering work by Schrauzer on TiO_2 in 1977[14], research efforts have intensified to develop efficient, stable, and cost-effective photocatalysts for driving this reaction under solar illumination. Nevertheless, their ammonia yields remain far below those achieved by the Haber-Bosch process. This stems mainly from the following severe challenges: (i) ultrafast recombination of photogenerated carriers results in most electrons being lost before they reach the surface[15,16], (ii) a single-component semiconductor can hardly satisfy both broad-spectrum light absorption and sufficient reduction driving force simultaneously, leading to poor solar energy utilization[17], (iii) the extreme inertness of the N≡N triple bond demands highly active chemisorption and electron-injection sites on the catalyst surface[8], (iv) the competing hydrogen evolution reaction (HER) almost always takes precedence in aqueous media, severely undermining the selectivity for nitrogen fixation[18], (v) Photocorrosion and structural instability limit the long-term use of many otherwise high-performance materials[19]. These challenges are intertwined and collectively hinder the practical application of photocatalytic nitrogen fixation.

To date, numerous photocatalysts have been developed, including oxides (e.g., WO_3[20,21], MnOx[22,23], CeO_2[24-26], *etc.*), sulfides (e.g., Bi_2S_3[27-29], $ZnCoS_x$[17,30], *etc.*), metal-organic frameworks (MOFs)[31-33], High-entropy alloys[34], and layered double hydroxides[35-37]. Among them, bismuth-based semiconductors (e.g., Bi_2O_3[38], BiOCl[39-41], Bi_2MoO_6[42-44], Bi-MOFs[45], *etc.*) demonstrate excellent visible light absorption, strong N_2 adsorption capacity, and eco-friendly properties, making them superior to traditional catalysts like TiO_2[46-48] and g-C_3N_4[49-52] in photocatalytic nitrogen fixation. To further enhance their performance, strategies such as defect engineering[53,54], elemental doping[55-57], and heterojunction construction[18] have been explored. Heterojunctions represent a pivotal structural strategy for enhancing catalytic performance, formed by integrating bismuth-based semiconductors with other semiconductors possessing matched or complementary work functions to create a synergistic composite system. It is worth mentioning that high-entropy materials often form dual-phase or multiphase structures, naturally generating abundant

heterojunction interfaces. This provides unique opportunities to regulate interfacial charge transfer and to activate the N≡N bond. Future research on bismuth-based heterojunctions could also benefit from coupling with high-entropy components to achieve enhanced synergistic photocatalysis.

Through precise interfacial engineering, heterojunctions improve catalytic behavior across multiple aspects: a built-in electric field and interfacial chemical bonding facilitate efficient charge-transfer channels, promoting directional separation and migration of photogenerated charge carriers while suppressing their recombination. Interfacial atomic reconstruction and electron redistribution further generate dedicated active sites, which strengthen the adsorption and activation of reactants and, collectively, lower the reaction energy barrier[58]. Moreover, appropriate energy-level alignment at the heterojunction integrates the light-harvesting properties of the individual semiconductors, broadening the photoresponse from the ultraviolet to the visible and even the near-infrared regions. When combined with interfacial plasmon resonance and light-scattering effects, this configuration enhances light absorption and increases the yield of photogenerated charges. Interfacial chemical bonding inhibits component dissolution, phase transformation, and aggregation, thereby extending catalyst durability[59]. Xu *et al.*[60] induce precisely controlled decomposition of the organic ligands in CoV-MOF, thereby creating abundant ligand defects and undercoordinated active sites within the metal-organic framework. These defect sites exhibit strong interactions with V^{5+} ions on the $BiVO_4$ surface, significantly enhancing the bonding strength of the interfacial V-O coordination bonds. This robust interfacial bonding effectively anchors V^{5+} ions in the $BiVO_4$ lattice, blocking the V^{5+} leaching pathway triggered by photogenerated holes and thus fundamentally suppressing vanadium ion dissolution and loss during the reaction. Lv *et al.*[61] constructed a Bi atomic-layer-bonded interface via an *in situ* anion exchange method. The O-Bi-S bonds at the interface provide a strong built-in electric field and efficient electron-transport channels, enabling the atomic-layer-bonded interface to serve as a charge-transfer pathway. This results in robust interfacial coupling and ultrahigh structural stability, effectively suppressing phase separation and component agglomeration during photocatalytic reactions. Redistribution of interfacial charge also helps moderate surface redox activity, thereby reducing photo-corrosion and chemical degradation and improving cycling stability[62].

This review systematically summarizes recent advances in Bi-based heterojunction photocatalysts for nitrogen fixation. Our discussion focuses on the critical role of interfacial engineering in Type-II, Z-scheme, and S-scheme heterojunctions, as well as strategies to enhance ammonia production through precise interfacial design. Finally, we discuss current challenges and future directions, providing a roadmap for developing efficient and sustainable bismuth-based photocatalysts for large-scale nitrogen fixation and a greener energy future.

MECHANISM INSIGHTS TOWARD PHOTOCATALYTIC NITROGEN FIXATION

Understanding how photocatalytic nitrogen fixation works is important for designing better catalysts. There are two main mechanisms: dissociation and association. In the dissociation mechanism, the strong N≡N triple bond breaks completely before any hydrogenation, producing individual nitrogen atoms that are then protonated. This method is used in the traditional Haber-Bosch process. However, at room temperature and atmospheric pressure, breaking the N≡N bond (which requires about 941 $kJ \cdot mol^{-1}$) is kinetically very difficult. For the Bi-based photocatalysts studied here, experiments and calculations indicate they favor an associative pathway rather than full dissociation. In this mechanism, the N-N single bond remains intact during the early hydrogenation steps, which can proceed along two different routes, as shown in Figure 1. One branch is the distal mechanism: the far nitrogen gets hydrogenated one step at a time, after which the N-N bond breaks. The other branch is the alternating mechanism, where both nitrogen atoms are hydrogenated in a stepwise fashion until the N-N bond finally cleaves, releasing two ammonia molecules[63,64].

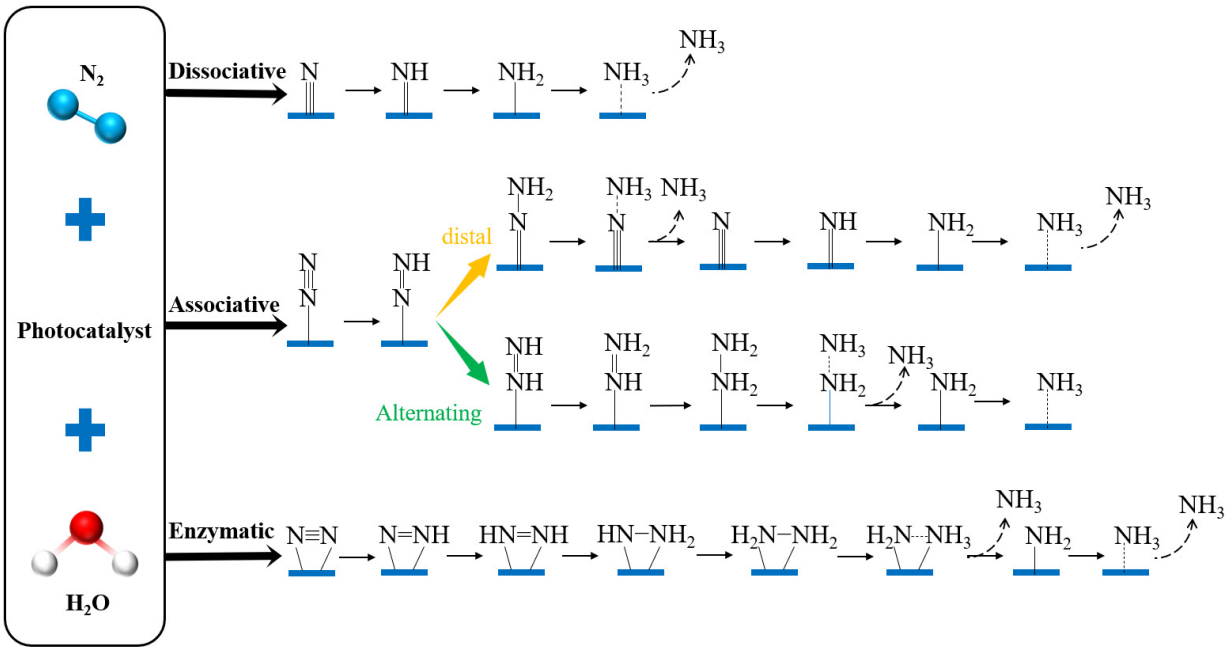

Figure 1. Various pathways for forming catalysts on photocatalysts.

The photocatalytic nitrogen fixation mechanism is initiated by the photoexcitation of electrons (e^-) from the valence band (VB) to the conduction band (CB) under solar irradiation, resulting in the formation of electron-hole (e^--h^+) pairs. Subsequently, the resulting charge carriers are separated and migrate to the catalyst surface. There, N_2 molecules are adsorbed onto active sites, such as metal centers, Lewis acid-base pairs, or defect sites. The adsorb N_2 subsequently undergoes multiple steps of proton-coupled electron transfer (PCET). The hydrogenation proceeds via a distal pathway, involving intermediates such as *NNH, *NNH2, *NH, *NH2, or via an alternating pathway, involving intermediates such as *NNH, *NHNH, *$NHNH_2$, *NH_2NH_2. Finally, upon desorption of the produced NH_3 from the catalyst surface, the active sites are regenerated, and the catalytic cycle can repeat[65,66]. In the photocatalytic nitrogen fixation process, the reduction potentials are required to generate key active intermediate sites, as shown in Figure 2. Bismuth-based semiconductor catalysts exhibit sufficiently negative reduction potentials to drive the critical formation of the *N_2H intermediate, a pivotal step in the Photocatalytic Nitrogen Fixation (PNF) pathway. The efficiency of this reaction can be further enhanced by optimizing the bandgap structure of bismuth-based photocatalysts (e.g., by reducing the bandgap), introducing structural defects such as oxygen vacancies (OVs), or increasing the density of surface-active sites[67,68].

RATIONAL DESIGN OF EFFICIENT PHOTOCATALYST FOR NITROGEN FIXATION

The design of high-performance photocatalytic nitrogen fixation catalysts requires integrating photocatalysis principles with nitrogen activation mechanisms to enhance solar energy utilization, strengthen nitrogen adsorption/activation, and improve product selectivity[69]. The successful formation of heterojunctions relies on both fundamental conditions. Fundamental prerequisites include selecting semiconductors with distinct physical properties and chemical compatibility[20]. Crystal structure matching is critical; mismatched structures can lead to defective interfaces or even prevent heterojunction formation. Moreover, the semiconductors must achieve intimate contact, ideally through epitaxial growth or other advanced synthesis techniques, to form a coherent and stable interface[69]. Ideal conditions include lattice matching and exposure of highly reactive crystal facets. Different crystal facets exhibit distinct atomic arrangements and electronic structures, significantly influencing catalytic behavior. Efficient charge-transfer channels can be established

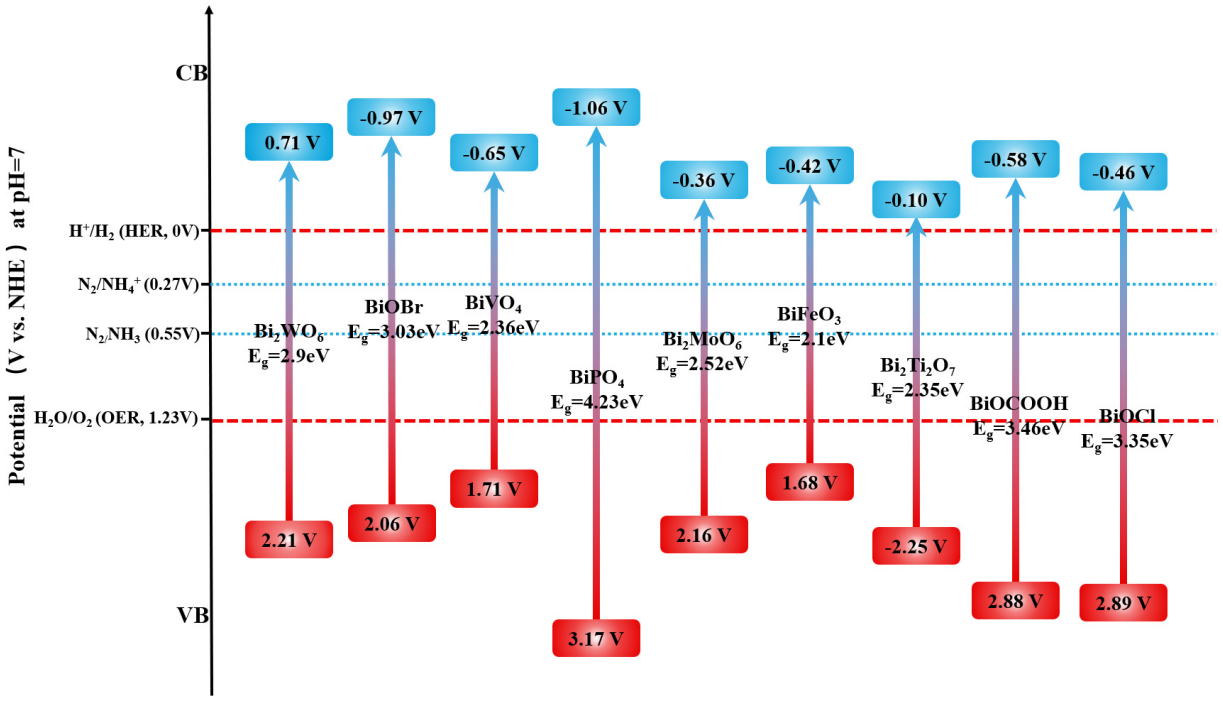

Figure 2. Energetic feasibility for N_2 reduction: conduction band positions of bismuth-based semiconductors against relevant redox couples. HER: Hydrogen evolution reaction; OER: oxygen evolution reaction; CB: conduction band; VB: valence band; NHE: normal hydrogen electrode.

between the two semiconductors by aligning their highly active crystal facets, thereby enhancing interfacial charge separation[70]. It is essential to form an atomically tight interface rather than simple physical mixing to avoid delamination or collapse during reactions, which would compromise the unique electronic structure and physicochemical properties that endow them with enormous application potential in photocatalysis, photo electrocatalysis, and other applications. In an ideal material pairing, at least one semiconductor should possess a strong visible-light absorption capacity to maximize solar energy harvesting[62]. Furthermore, the heterojunction structure should be designed to improve overall chemical stability and anti-photo corrosion properties[20].

Crystal engineering and architectural design of Bi-based catalysts

Bismuth-based catalysts have attracted significant attention due to their applications in energy-related fields. Based on their crystal structures, these catalysts can be primarily classified into four categories.

Layer-like structural bismuth oxyhalides

Layered bismuth oxyhalides (commonly denoted as BiOX, where X = Cl, Br, I) are typical representatives of this structural family. Their crystal structure consists of alternating cationic $Bi_2O_2^{2+}$ layers and anionic halogen ion (X^-) slabs[71], which are stacked through weak van der Waals interactions, as shown in Figure 3A. This structural configuration yields a relatively high specific surface area along with abundant exposed active sites. Meanwhile, the band gap progressively narrows as the atomic number of the halogen increases (Eg, BiOCl > BiOBr > BiOI), thereby enhancing visible-light absorption. Notably, the weak interlayer bonding allows facile modification of bismuth oxyhalides through strategies such as ion exchange or intercalation (e.g., incorporation of organic molecules or metal nanoparticles). Moreover, an intrinsic static electric field is established between the positively charged $Bi_2O_2^{2+}$ layers and the negatively charged X^- layers[39], which facilitates the separation of photogenerated electrons (e^-) and holes (h^+) while suppressing their

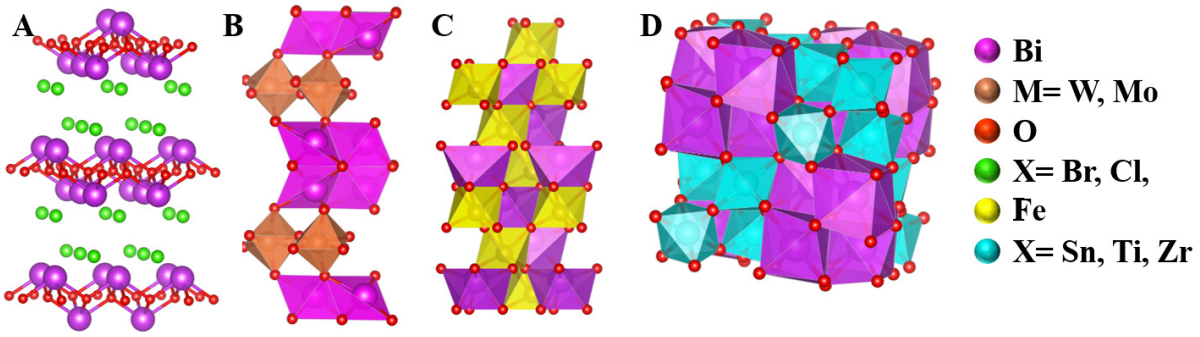

Figure 3. Typical crystal structure and energy-band structures of key bismuth-based catalysts. (A) Perovskite-like layered structure of BiOX (X = Cl, Br, I), (B) Bi_2MO_6 (M = W, Mo), (C) ABO_3, (D) $Bi_2X_2O_7$ (X = Sn, Ti, Zr).

recombination. Charge transport exhibits strong anisotropy: electrons migrate predominantly within the layers (perpendicular to the c-axis), whereas holes transport across the interlayer space, thereby improving charge carrier utilization efficiency. The layered architecture of bismuth oxyhalides offers versatile routes for material engineering, including heterojunction construction, surface defect incorporation, and morphological nanostructuring[72,73].

Perovskite-like structural Bi-based semiconductor

Bi_2MoO_6 and Bi_2WO_6 are layered Aurivillius-type oxides, consisting of alternating stacks of positively charged $Bi_2O_2^{2+}$ layers and perovskite-like MO_6^{6-} slabs (M = Mo, W), as shown in Figure 3B. The $6s^2$ lone-pair electrons of Bi^{3+} ions, being stereochemically active, give rise to spontaneous polarization, generating a strong internal electric field between the layers. This built-in field effectively promotes the unidirectional separation of photogenerated charge carriers, with electrons moving toward the perovskite-like slabs and holes toward the $Bi_2O_2^{2+}$ layers, thereby significantly suppressing recombination[74]. These materials exhibit a moderate band gap (approximately 2.4-2.9 eV), providing good visible-light absorption. The weak interlayer interactions facilitate interlayer charge transfer, enabling fast movement of photogenerated electrons from the perovskite-like slabs toward surface N_2 adsorption sites and reducing carrier recombination. The layered architecture provides abundant surface-active sites, and hybridization between Bi 6s and N 2p orbitals improves the kinetics of nitrogen chemisorption and activation. Specifically, in Bi_2MoO_6, significant distortion of the MoO_6 octahedra synergizes with the lone pair effect of Bi^{3+}, reinforcing the internal electric field[42]. In Bi_2WO_6, the distortion of the WO_6 octahedra is less pronounced; however, its ultrathin nanosheet morphology shortens charge migration pathways, further suppressing bulk recombination and exposing more active facets. Although interlayer coupling is relatively strong, strategies such as constructing heterojunctions can effectively tailor their catalytic performance[75].

Bismuth-based perovskite-structured semiconductors

Perovskites have the general formula ABO_3, as shown in Figure 3C. In bismuth-based catalysts, bismuth (Bi) can occupy different sites (e.g., $Bi_{0.5}Na_{0.5}TiO_3$ and $SrBiO_3$). In either position, its inclusion fundamentally alters the material's intrinsic properties. The bismuth ion (Bi^{3+}) has a stereochemically active $6s^2$ lone pair of electrons. At the A-site, this lone pair induces pronounced local lattice distortion, breaking centrosymmetry. The distortion can generate internal electric fields and destabilize lattice oxygen, promoting oxygen vacancy formation. When bismuth occupies the B-site in higher valence states (e.g., Bi^{4+}/Bi^{5+}), it acts as a direct catalytic center. The Bi^{3+}/Bi^{5+} redox couple provides efficient electron-transfer pathways for reactions. Notably, some bismuth-based perovskites (e.g., $BiFeO_3$[76,77]) may undergo surface corrosion under mild conditions, leading to bismuth dissolution and the *in situ* formation of a highly active (hydr)oxide layer. This

self-reconstruction creates a core-shell architecture: a stable perovskite core serves as a conductive skeleton, while the surface (hydr) oxide provides abundant active sites.

Pyrochlore structural bismuth-based semiconductor

Pyrochlore-structured materials, exemplified by $Bi_2X_2O_7$ (X = Sn, Ti, Zr), feature a three-dimensional network composed of alternating $Bi_2O_2^{2+}$ layers and oxygen-based anionic groups, as shown in Figure 3D. In this structure, Bi^{3+} ions adopt an eight-coordinate geometry, while X^{4+} ions occupy distinct crystallographic sites[78-81]. The good match in ionic radii between the cations, combined with their linkage via oxygen bridges, confers excellent thermal and chemical stability to the framework. These materials exhibit a moderate band gap (typically 2.0-3.0 eV), fulfilling essential criteria for photocatalytic nitrogen fixation. Cation vacancies and a continuous oxygen-coordination network serve as efficient pathways for the transport of photogenerated electrons. Oxygen vacancies, as a prominent type of surface defect, function as active sites for nitrogen adsorption and activation. They promote N≡N bond cleavage by destabilizing the triple bond, thereby reducing the kinetic barrier for subsequent reduction[82]. Furthermore, pyrochlore-type compounds are often coupled with semiconductors such as TiO_2 and g-C_3N_4 to form heterojunctions[83,84]. This approach extends the light-harvesting range and leverages the interfacial internal electric field to promote charge separation, leading to enhanced.

Overall photocatalytic efficiency. The structure also exhibits considerable tolerance to doping and defects, allowing its electronic structure and catalytic activity to be systematically tuned through compositional design.

Interface engineering in bismuth-based heterojunctions

Interface engineering is a pivotal strategy for optimizing the nitrogen-fixation performance of bismuth-based photocatalysts. By precisely tailoring the structure, electronic states, and interactions at heterojunction interfaces, it systematically addresses critical challenges, including inefficient carrier separation and inadequate N_2 activation. The primary roles of interface engineering can be summarized as follows: (i) Facilitating charge separation and migration: Intrinsic electric fields or directional charge-transport pathways are established at the interface, enabling the spatial decoupling of photogenerated charge carriers and their accumulation at nitrogen-reduction and water-oxidation sites, respectively[85]; (ii) enhancing N_2 adsorption and activation: The interfacial chemical microenvironment is optimized to enhance N_2 binding and destabilize the N≡N triple bond, thereby lowering the activation energy barrier[86]; (iii) improving interfacial charge-transfer kinetics: Intimate interfacial contact reduces the barrier to charge transfer and considerably facilitates carrier transport across the interface[87,88]; (iv) increasing structural stability: Interfacial modification or composite formation suppresses the loss or deactivation of active components, extending the operational lifetime of the catalyst[89].

The routes for improving the nitrogen fixation performance of bismuth-based photocatalysts through interface engineering include: (i) Controlled introduction of defects, especially OVs[90-92], which modulate interfacial electronic states and adsorption behavior. OVs shift the conduction band minimum (CBM) of bismuth-based semiconductors negatively, improve N_2 reduction capability, and induce localized charge accumulation that reinforces the built-in electric field. Defect sites also serve as selective adsorption centers for N_2, lengthening the N≡N bond and lowering the activation barrier. Synergy between defects and Bi^{3+} sites creates dual-active centers. Simultaneously, shortened charge-transfer pathways caused by defects and increased band bending further inhibit carrier recombination. While oxygen vacancy engineering can significantly enhance light absorption, charge separation, and small-molecule activation in bismuth-based photocatalysts, excessive oxygen vacancy concentrations lead to significant lattice distortion and diminished

crystallinity. Under such conditions, an overabundance of defects can serve as centers for recombination of photogenerated carriers, intensifying electron-hole recombination and decreasing charge-migration efficiency. Additionally, a high density of oxygen vacancies compromises the material's structural stability, making the vacancies more prone to filling, which can lead to corrosion and catalyst deterioration. It also disrupts band energy alignment, weakening the driving force for redox reactions. Ultimately, these negative effects collectively result in a comprehensive decline in catalytic activity, selectivity, and cycling stability[93]; (ii) Interfacial chemical bonding[58,94].Constructing atomically precise chemical linkages across the interface creates "barrier-free" charge-transfer channels, lowering the energy barrier for carrier migration. The reinforced built-in electric field enables oriented charge flow and improves interfacial stability. Chemical bonds can also engage in secondary interactions with reaction intermediates (e.g., $*N_2$, *NNH, $*NH_2$), stabilizing transition states and reducing the energy barriers of hydrogenation steps. Moreover, chemically bonded proton-transfer pathways facilitate H^+ delivery to active sites; (iii) Interfacial heteroatom doping[44]. Introducing metal or non-metal heteroatoms tunes the interfacial electronic structure and the distribution of active sites. Metal dopants introduce electrons into the N_2 antibonding orbitals[39], compromising the N≡N bond, while non-metal atoms form covalent bonds that adjust local charge density. Furthermore, metal sites can create additional active centers that cooperate with Bi^{3+}, whereas non-metal atoms help anchor OVs, preventing their aggregation and enhancing N_2 adsorption. Doping also introduces defect levels that broaden light absorption and optimize band alignment.

Design and construction of Bi-based heterojunction

Constructing heterojunctions effectively promotes charge separation and migration in bismuth-based photocatalysts[95]. By coupling semiconductors with different Fermi level (EF), spontaneous electrons transfer from the lower work function (or ionization energy)[96]. Common types of heterojunctions encompass conventional, Z-scheme, and S-scheme heterojunctions. Traditional heterojunction photocatalysts are typically categorized into three groups, as shown in Figure 4A-C: Type-I (straddling gap), Type-II (staggered gap), and Type-III (broken gap). In traditional heterojunctions, the Type-I structure tends to promote charge recombination due to carrier confinement[97]. In contrast, the Type-III configuration, with its non-overlapping band structures, hinders interfacial charge transfer and cooperative redox reactions. In contrast, the Type-II heterojunction stands out as the most effective approach, as its structure facilitates the spatial separation of electron-hole pairs, thereby enhancing photocatalytic activity[98]. Upon photoexcitation of the Z-scheme heterojunction, electrons and holes are generated in the CB and VB of both photocatalyst II (PS II) and photocatalyst I (PS I)[99]. The photogenerated electrons in the CB of PS II then migrate to the VB of PS I via redox shuttles. This transfer results in the retention of highly oxidizing holes in the VB of PS II and highly reducing electrons in the CB of PS I, as shown in Figure 4D. These charge carriers can subsequently drive oxidation and reduction reactions on the photocatalyst surface[100]. In an S-scheme heterojunction, an oxidation semiconductor (OP) is coupled with a reduction semiconductor (RP), as shown in Figure 4E. The difference in their EF causes electrons from the RP to migrate toward the OP at the interface. When equilibrium is reached, the OP becomes negatively charged and the RP positively charged. This process leads to band bending at the interface and generates an internal electric field between the two semiconductors. Consequently, the combined action of the internal electric field and band bending prevents electrons from the RP's conduction band from flowing into the OP's conduction band, thereby facilitating the spatial separation of the electron-hole pairs[101-104].

Type-II heterojunction

In a Type II heterojunction, the energy bands of the two semiconductors are staggered, creating a mismatched alignment. Photogenerated electrons tend to move from the semiconductor with a higher CBM to the one with a lower CBM. Conversely, photogenerated holes migrate from the semiconductor with a lower valence band maximum (VBM) to the one with a higher VBM. This spatial separation of charges

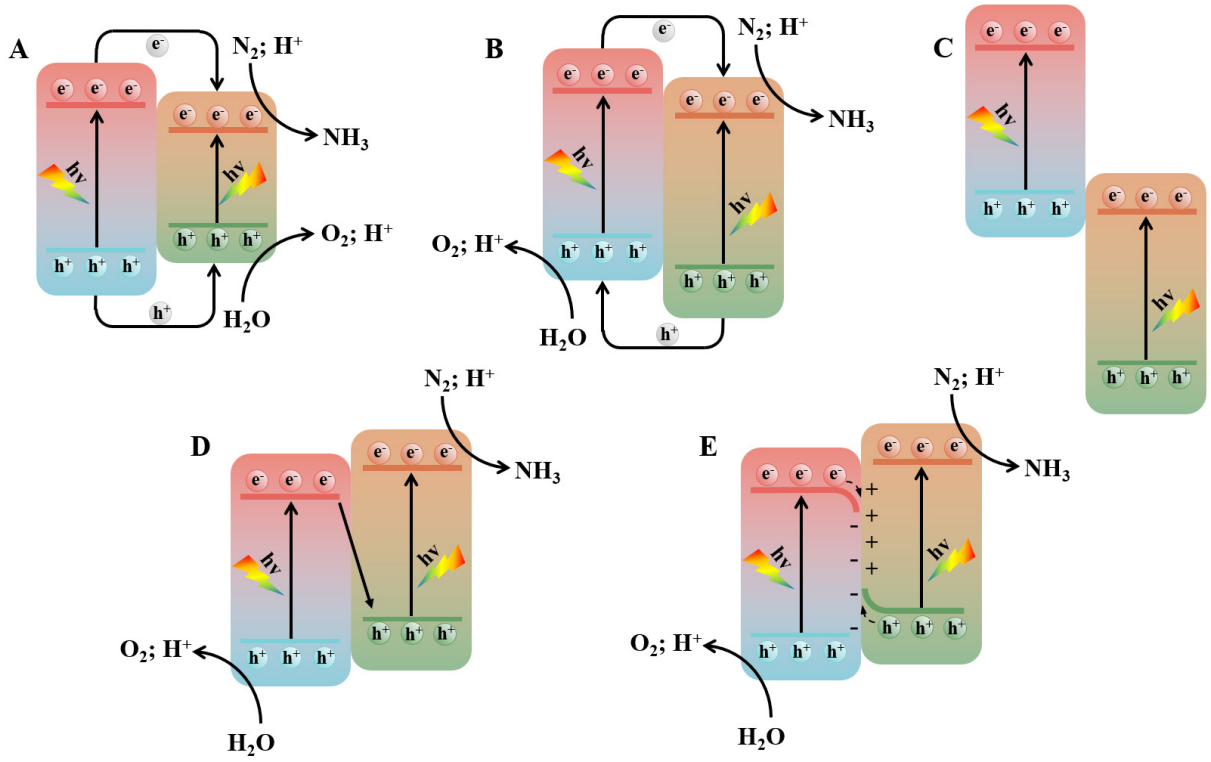

Figure 4. (A) Type-Ⅰ heterojunction; (B) Type-II heterojunction; (C) Type-Ⅲ heterojunction; (D) Z-scheme heterojunction; (E) S-scheme heterojunction.

effectively reduces bulk recombination of electron-hole pairs and markedly extends carrier lifetimes - an important benefit of Type II heterojunctions in photocatalytic applications.

However, this charge separation incurs a reduction in some redox potential. Specifically, electrons localize on the semiconductor with a higher CBM (indicating a weaker reduction ability), while holes accumulate on the semiconductor with a lower VBM (indicating a weaker oxidation ability). Consequently, electrons and holes tend to become confined at sites where their reducing and oxidizing capabilities are comparatively limited. This results in a decreased driving force per charge carrier, despite an increased number of carriers available for surface reactions. Therefore, designing a Type II heterojunction requires balancing charge-separation efficiency with maintaining adequate redox potentials. When the band alignment of the two semiconductors is properly matched - even if electrons transfer to a slightly less favorable reduction site - the conduction band minimum can still be positioned above the thermodynamic potential needed for specific reactions such as N_2 reduction to NH_3[37]. In this case, photocatalytic efficiency is greatly enhanced while ensuring the reaction proceeds.

Constructing a Type-II heterojunction requires precise calculation and design of the band positions of the two semiconductors to achieve an ideal staggered alignment. Moreover, it is essential to form intimate, large-area heterointerfaces, such as core-shell structures or layered composites, to provide ample channels for the directional migration of electrons and holes. The synthesis process must be finely controlled to minimize interfacial defects, since the core of interface engineering in Type-II heterojunctions lies in ensuring good physical contact and proper band alignment while suppressing interfacial defects[101]. Table 1 summarizes data on type-II heterojunctions over the past few years.

Table 1. Bi-based type-II heterojunction for N_2 reduction to NH_3

Photocatalyst	Light source	Scavenger	Performance ($\mu mol \cdot g^{-1} \cdot h^{-1}$)	Catalyst loading (mg)	Reaction volume (mL)	Ref.
Vo-$Bi_{12}O_{17}Br_2$/ZnCr-LDHs	300 W Xe lamp	H_2O	286.0	50	100	[37]
$Bi_4O_5Br_2$/$CdWO_4$	300 W Xe lamp	CH_3OH/H_2O	501	100	200	[105]
α-Bi_2O_3-Bi_3O_4Br	300 W Xe lamp	CH_3OH/H_2O	238.7	15	15	[106]
Bi@BiOBr–Bi_2MoO_6	300 W Xe lamp	H_2O	167.2	10	100	[107]
BrO_3^--Bi_2O_3/$Bi(OH)_3$	300 W Xe lamp	H_2O	45.28	50	100	[108]
$KNbO_3$/$Bi_4O_5Br_2$	300 W Xe lamp	CH_3OH/H_2O	89.4	100	100	[109]
g-C_3N_4/Bi_2MoO_6	500 W Xe lamp	C_2H_5OH/H_2O	1,090	40	40	[110]
$BiPO_4$/$Bi_4O_5Br_2$	300 W Xe lamp	CH_3OH/H_2O	370	100	100	[111]
$Bi_{12}O_{17}Cl_2$/BiOCOOH/Bi_2MoO_6	300 W Xe lamp	H_2O	107.78	15	15	[112]
BiOBr-Vo/MIL-101(Fe)-F	300 W Xe lamp ($\lambda \geq 420$ nm)	H_2O	80.9	2	5	[113]

$BiPO_4$ is a low-cost, non-toxic, and chemically stable Ultraviolet-Visible (UV)-responsive photocatalyst with activity surpassing that of TiO_2. It has been widely employed as a cocatalyst to promote charge separation in a heterostructure. Zhao *et al.*[111] synthesized a $BiPO_4$/$Bi_4O_5Br_2$ composite photocatalyst via a simple solvothermal method, constructing a Type II heterojunction at the interface. Due to the higher Fermi level of $BiPO_4$ compared to $Bi_4O_5Br_2$, electron transfer from $BiPO_4$ to $Bi_4O_5Br_2$ occurs upon contact, resulting in negative charge accumulation in the interfacial region of $Bi_4O_5Br_2$ and positive charge in $BiPO_4$. The charge redistribution establishes a built-in electric field that enables directional migration of photogenerated carriers, as shown in Figure 5A, thereby achieving efficient spatial separation of electron-hole pairs. As a key Bi-based semiconductor, $Bi_4O_5Br_2$ features a layered structure composed of alternating $[Bi_2O_2]^{2+}$ and halogen-ion layers, which generates a built-in electric field along the c-axis that promotes charge separation upon photogeneration. Nonetheless, rapid carrier recombination in pure $Bi_4O_5Br_2$ limits the availability of electrons for nitrogen reduction, constraining its nitrogen fixation performance. To address this, Yue *et al.*[109] Fabricated a $KNbO_3$/$Bi_4O_5Br_2$ heterojunction by embedding $KNbO_3$ microcubes into $Bi_4O_5Br_2$ nanosheets via a combined hydrothermal - precipitation approach, achieving intimate interfacial contact. The resulting charge redistribution induces downward band bending in $Bi_4O_5Br_2$ and an upwardly bent band structure in $KNbO_3$, which facilitates electron transfer from the CB of $Bi_4O_5Br_2$ to that of $KNbO_3$, and holes from the VB of $KNbO_3$ to that of $Bi_4O_5Br_2$, as shown in Figure 5B, thereby enabling efficient spatial separation of electron-hole pairs.

Other bismuth-based semiconductors, such as BiOBr, Bi_2WO_6, Bi_2MoO_6, and $Bi(OH)_3$, have also shown promise in photocatalysis. Among them, bismuth hydroxide [$Bi(OH)_3$] exhibits notable activity, but its wide bandgap (3.40 eV) restricts light absorption to the UV region. To address this, Liu *et al.*[108] synthesized a BrO_3^--bridged Bi_2O_3/$Bi(OH)_3$ heterojunction via a hydrothermal method under strongly alkaline conditions. At the interface, BrO_3^- forms a Bi-BrO_3^--O-Bi structure that serves as an effective charge-transfer bridge. This configuration captures photogenerated electrons from the conduction band of Bi_2O_3, facilitating the reduction of Br and increased local electron density, as shown in Figure 5C. Consequently, charge transport resistance is reduced, and interfacial charge-transfer efficiency is significantly enhanced. Cao *et al.*[112] constructed a ternary $Bi_{12}O_{17}Cl_2$/BiOCOOH/Bi_2MoO_6 heterojunction via a one-step synthesis under mild conditions, achieving both heterojunction formation and the introduction of oxygen vacancies. $Bi_{12}O_{17}Cl_2$ nanoparticles are uniformly deposited onto the precursor surface without altering its morphology, forming an intimate interfacial contact with no physical gaps. In term of charge transfer, electrons migrate sequentially from the CB of Bi_2MoO_6 to those of BiOCOOH and $Bi_{12}O_{17}Cl_2$ in a stepwise energy increase,

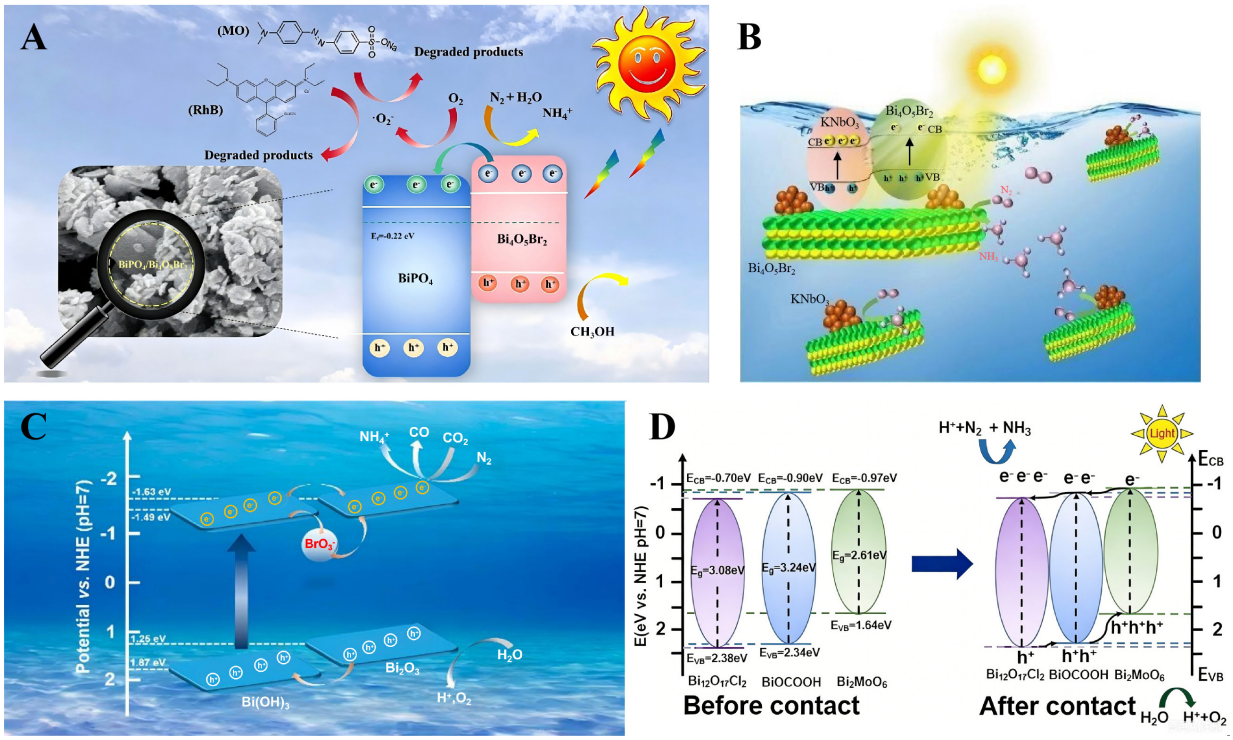

Figure 5. (A) Photocatalytic mechanisms of $BiPO_4/Bi_4O_5Br_2$. (Reproduced with permission from[111], Copyright 2023, Elsevier); (B) Photocatalytic mechanisms of $KNbO_3/Bi_4O_5Br_2$. (Reproduced with permission from[109]. Copyright 2024, Higher Education Press and Springer Nature; (C) Photocatalytic mechanisms of BrO_3^--bridged $Bi_2O_2/Bi(OH)_2$. (Reproduced with permission from[108]. Copyright 2023, American Chemical Society; (D) Photocatalytic mechanisms of $Bi_{12}O_{17}Cl_2/BiOCOOH/Bi_2MoO_6$. (Reproduced with permission from[112]. Copyright 2024, Elsevier). NHE: Normal hydrogen electrode.

while holes transfer in the reverse direction, moving from the VB of $Bi_{12}O_{17}Cl_2$ to BiOCOOH and Bi_2MoO_6, enabling effective spatial separation of charge carriers., enabling effectively spatial separation of charge carriers, as shown in Figure 5D.

Using an *in-situ* solvothermal approach, Xue *et al.*[114] decorated Bi_2MoO_6 nanorods with oxygen vacancy-rich p-type BiOBr nanosheets (OV-BiOBr), forming a hierarchical "nanorod-nanosheet" heterointerface, as shown in Figure 6A-C. The close contact between crystal facets and the type-II band alignment achieved through p-n junction engineering facilitates the migration of photogenerated electrons from the CB of Bi_2MoO_6 to that of OV-BiOBr and the migration of holes from the valence band of OV-BiOBr to that of Bi_2MoO_6, significantly suppressing electron-hole recombination. Moreover, the introduced OVs serve as electron traps at the interface, capturing transferred electrons and further reducing charge recombination, as shown in Figure 6D. Zhao *et al.*[105] synthesized $Bi_4O_5Br_2/CdWO_4$ composite via a two-step hydrothermal method, ensuring intimate interfacial contact rather than simple physical mixing. The resulting charge redistribution is accompanied by upward band bending in $CdWO_4$ and downward band bending in $Bi_4O_5Br_2$. This synergistic alignment greatly enhances the transfer of photogenerated electrons from the conduction band of $Bi_4O_5Br_2$ to that of $CdWO_4$ while promoting hole migration from the valence band of $CdWO_4$ to the valence band of $Bi_4O_5Br_2$, resulting in efficient spatial separation of charge carriers, as illustrated in Figure 6E. The type-II heterojunction also minimizes electron-hole recombination, which is supported by increased photocurrent, lowered charge-transfer resistance observed in electrochemical impedance spectroscopy, and notable suppression of photoluminescence emission, as depicted in Figure 6F-H.

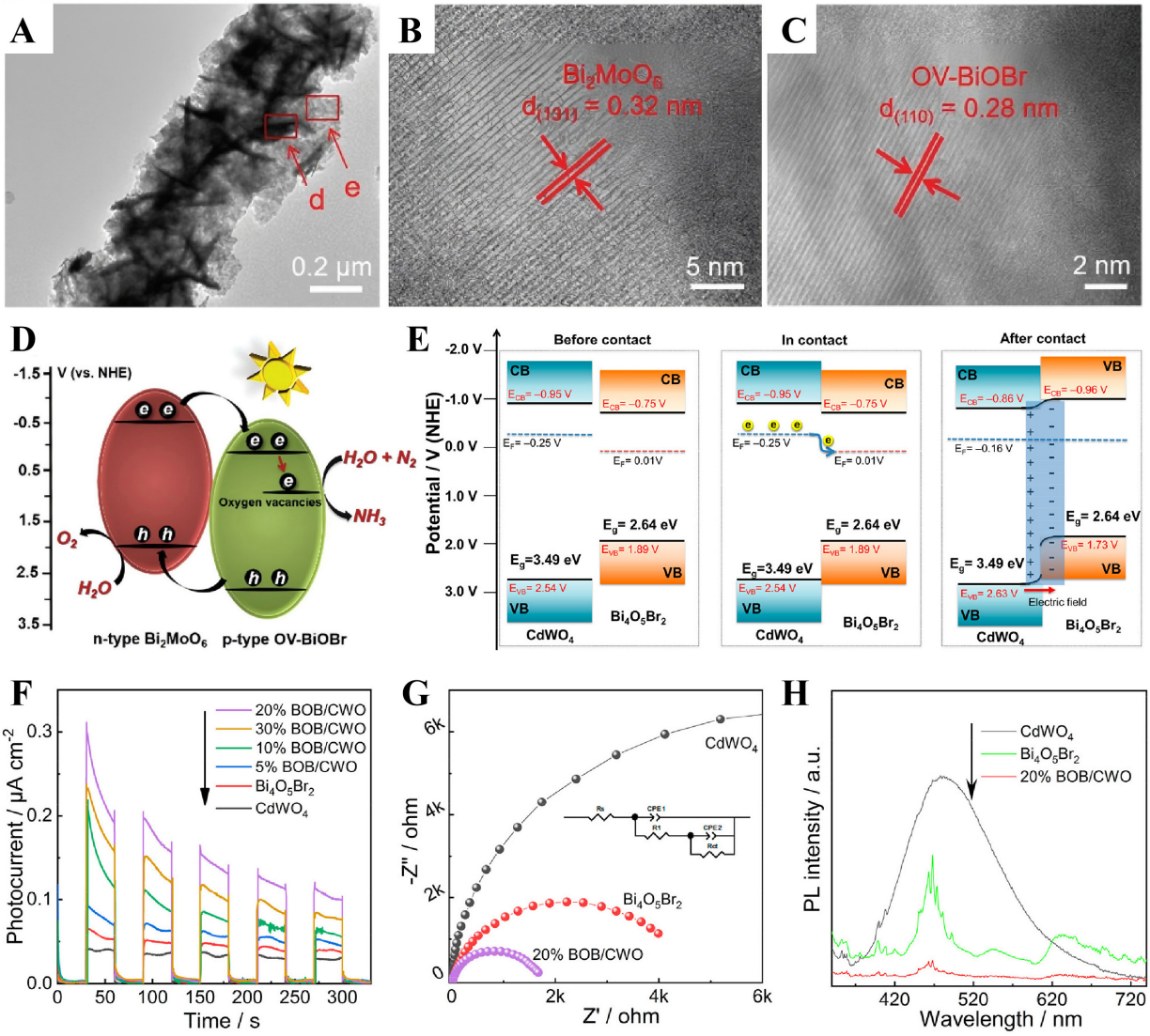

Figure 6. (A) Transmission electron microscopy (TEM) and (B and C) High-resolution TEM (HRTEM) images of Bi_2MoO_6/OV-BiOBr p-n heterojunctions; (D) The proposed reaction mechanism of photocatalytic N_2 fixation over Bi_2MoO_6/OV-BiOBr heterojunctions. (A-D) Reproduced with permission from[114]. Copyright 2019, Royal Society of Chemistry; (E) band diagrams of $CdWO_4$ and $Bi_4O_5Br_2$. Transient photocurrent response (F), EIS plots (G), and photoluminescence (PL) spectra (H) of $CdWO_4$, $Bi_4O_5Br_2$, and $Bi_4O_5Br_2$/$CdWO_4$ composites. (E-H) Reproduced with permission from[105]. Copyright 2023, American Chemical Society. CB: Conduction band; VB: valence band; BOB: BiOBr; CWO: $CdWO_4$; EIS: electrochemical impedance spectroscopy; NHE: normal hydrogen electrode.

Overall, Type-II heterojunctions offer a straightforward and effective interface engineering approach to spatially separate photogenerated carriers, although this may slightly weaken redox potentials. Their performance depends critically on close interfacial contact, staggered band alignment, and suppression of interfacial defects, which together improve the availability of electrons for nitrogen reduction.

Z-type heterojunction

In the Z-scheme heterojunction structure, photogenerated electrons (e^-) accumulate in the CB of one component and engage in reduction half-reactions. Since the conduction band position of this component is higher than that of the other, these electrons have a stronger reduction potential. As a result, bismuth-based Z-scheme heterojunctions generally demonstrate superior photocatalytic reduction performance compared to type-II heterojunctions, making them a primary focus in photocatalytic nitrogen fixation. Although less

Table 2. Bi-based Z-scheme heterojunction for N_2 reduction to NH_3

Photocatalyst	Light source	Scavenger	Performance ($\mu mol \cdot g^{-1} \cdot h^{-1}$)	Catalyst loading (mg)	Reaction volume (mL)	Ref.
$Bi/Bi_2S_3/SnS_2$	300 W Xe lamp	H_2O	96.4	20	100	[29]
$\beta Bi_2O_3/BiOCOOH$	300 W Xe lamp	CH_3OH/H_2O	65.56	15	15	[38]
$BiVO_4/ZnIn_2S_4$	300 W Xe lamp	H_2O	80.6	50	200	[91]
$Bi_2MoO_6/g\text{-}C_3N_4$	300 W Xe lamp	H_2O	227.8	50	100	[116]
$BiOBr/Bi_4O_5Br_2$	300 W Xe lamp	H_2O	66.87	50	100	[117]
$Bi\text{-}Bi_2O_3/KTa_{0.5}Nb_{0.5}O_3$	300 W Xe lamp	CH_3OH/H_2O	466.2	50	100	[118]
$KBiFe_2O_5/BiOBr$	300 W Xe lamp	H_2O/isopropanol	1,500	25	25	[119]
$GQDs/g\text{-}C_3N_4/BiOCl$	300 W Xe lamp	CH_3OH/H_2O	1,773.8	20	50	[120]
$Cu_2O/BiFeO_3@Ti_3C_2$ MXene	300 W Xe lamp	H_2O	366	50	100	[121]
BiOCl/NMT	300 W Xe lamp	H_2O	88.6	50	100	[122]
$Cu/WO_2/C\text{-}BiOBr$	300 W Xe lamp	H_2O	477.5	10	100	[123]
$Cu_2O@BiOCl$[100]	300 W Xe lamp	H_2O	181.9	50	200	[124]
$Bi_2O_3@CoAl\text{-}LDHs$	300 W Xe lamp	Na_2SO_3 solution	48.7	50	150	[125]
ZnO/Bi_2O_4	300 W Xe lamp	CH_3OH/H_2O	220	50	50	[126]

structurally complex than type-II heterojunctions, Z-scheme heterojunctions still necessitate close contact between the semiconductors and the intermediate conductor to facilitate effective electron transfer. The core strategy in interface engineering for Z-scheme heterojunctions is therefore to construct a conductive "bridge" that directs the selective recombination of charge carriers. This mechanism ensures the spatially directed recombination of less active charge carriers, thereby retaining holes with the highest oxidation potential in the component with a lower valence band position, and electrons with the highest reduction potential in the component with a higher conduction band position[115]. Table 2 summarizes data on Z-type heterojunctions over the past few years.

Liu *et al.*[56] directly anchored 2D boron-doped graphene quantum dots (BGQDs) onto the surface of 3D Bi_2MoO_6 (BMO) microspheres using an *in-situ* growth method, forming a closely integrated "quantum dot-microsphere" structure, as shown in Figure 7A-C. The BGQDs are bonded to surface atoms of BMO via chemical bonds, such as B-C and B-O, thereby avoiding interface detachment issues associated with physical mixing. The interfacial chemical bonding also suppresses the agglomeration tendency of BGQDs, as shown in Figure 7D-F. Even when the loading of BGQDs is increased to 30%, only a slight performance decline is observed, without severe light-blocking. Cao *et al.*[116] utilized interlayer van der Waals forces to spontaneously form a 2D/2D stacked heterojunction of $Bi_2MoO_6/g\text{-}C_3N_4$ (BMO/CN). This process requires no additional binders or high-temperature treatment, thereby avoiding interface contamination and structural damage, and ensuring the cleanliness and integrity of the interface. Differential charge density calculations reveal significant charge redistribution at the CN-BMO interface, as shown in Figure 7G. Bader charge analysis indicates that approximately 0.92 e is transferred from CN to BMO, confirming the directionality of electron transfer at the interface. The bridging N atoms of CN at the interface serve as electron migration channels, facilitating efficient interfacial charge transport, as shown in Figure 7H-I.

Noble metals (e.g., Pt, Au, Ag) have been widely used as electron mediators in traditional Z-scheme heterojunction photocatalysts[12,127,128] but these are costly and hinder large-scale applications. Moreover, in photocatalytic nitrogen fixation, the HER strongly competes with the nitrogen reduction reaction (NRR), thereby reducing the efficiency of NH_3 production. To address these issues, Chen *et al.*[118] Co-deposited Bi metal and Bi_2O_3 onto the surface of $KTa_{0.5}Nb_{0.5}O_3$ (KTN) via a one-step solvothermal method, forming a

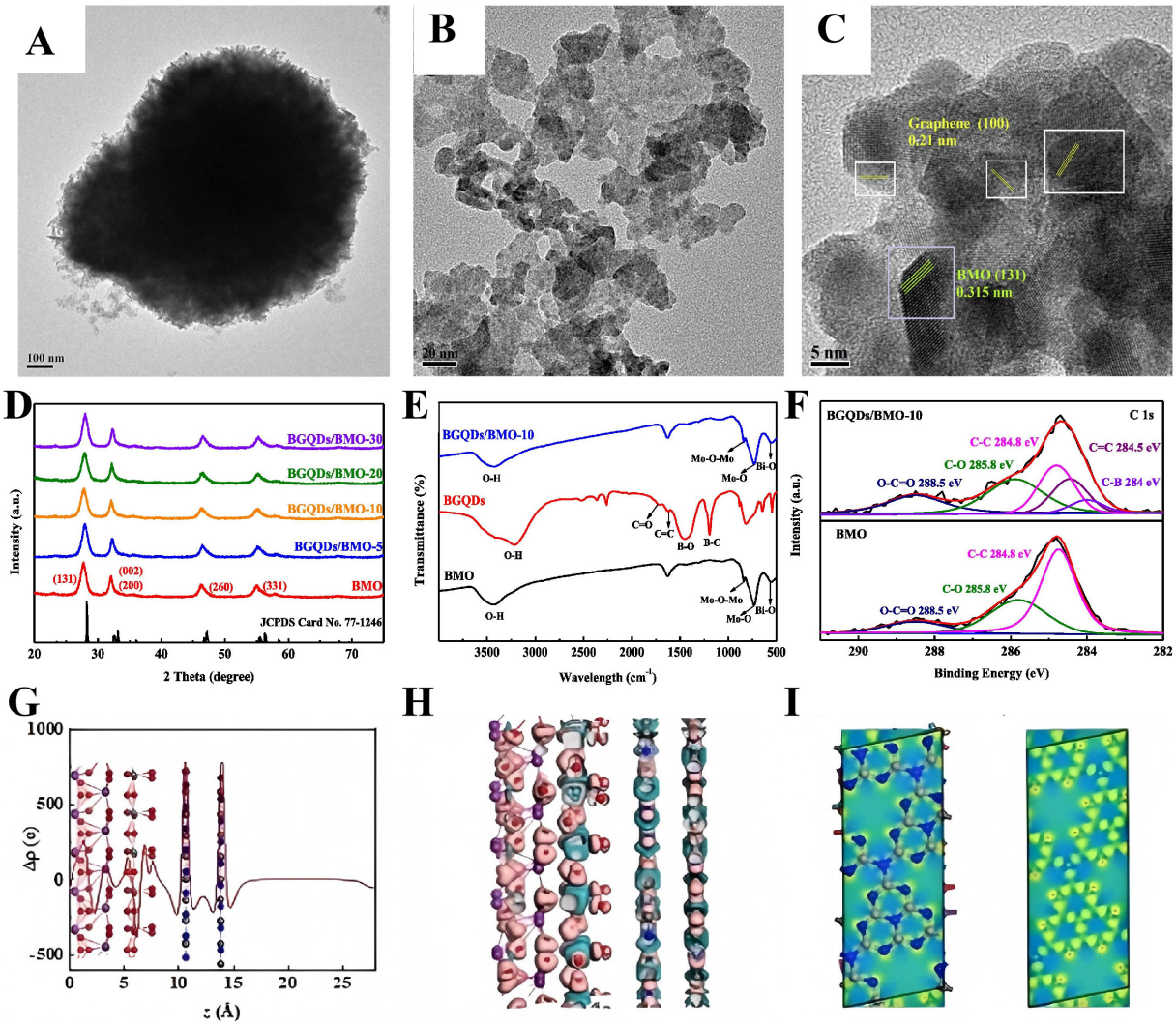

Figure 7. (A and B) TEM images of BGQDs/BMO. (C) HRTEM image of BGQDs/BMO. (D) XRD patterns of BMO and BGQDs/BMO. (E) Fourier transform infrared spectra of BGQDs, BMO, and BGQDs/BMO. (F) XPS C1S spectra of BMO and BGQDs/BMO. (A-F) Reproduced with permission from[56]. Copyright 2023, Elsevier; (G) Planeaveraged differential charge density. (H) Charge density distribution of CN-BMO. (I) The slice of charge density distribution of CN-BMO. (G-I) Reproduced with permission from[116]. Copyright 2024, Elsevier. TEM: Transmission electron microscopy; HRTEM: high-resolution TEM; BGQDs: boron-doped graphene quantum dots; BMO: Bi_2MoO_6; XRD: X-ray powder diffraction; XPS: X-ray photoelectron spectroscopy.

Bi-Bi_2O_3/KTN ternary composite system, rather than a modification with only Bi or Bi_2O_3. The incomplete core-shell structure plays a key interfacial role, as shown in Figure 8A and B. It ensures compatibility between KTN and Bi_2O_3, while the exposed Bi metal serves as active sites for N_2 adsorption, suppresses HER, and enhances NRR. Upon photoexcitation, electrons from the CB of $Bi_2O_3$are transferred through the Bi metal bridge to the VB of KTN, where they recombine with holes. Meanwhile, the electrons retained in the conduction band of KTN participate in N_2 reduction, as shown in Figure 8C. Through tailoring the composition and structure of the interface, the selectivity of interfacial reactions is improved. Owing to its high hydrogen adsorption energy and low HER activity, the exposed Bi metal suppresses the reduction of H^+ to H_2 at the interface, thereby minimizing competitive H_2 evolution against NRR. Moreover, Bi metal can effectively adsorb and activate the N≡N triple bond. Through its synergistic interaction with KTN, the energy barrier for N_2 reduction is lowered.

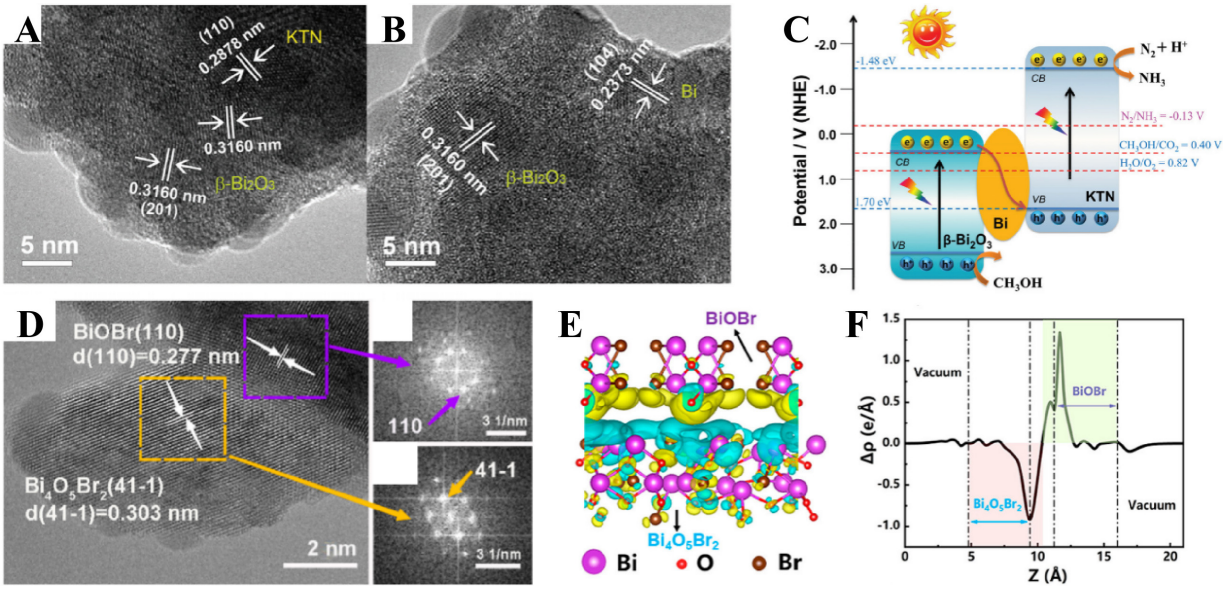

Figure 8. (A and B)TEM images, (C) band structure diagram of Bi-Bi_2O_3/KTN. (A-C) Reproduced with permission from[118]. Copyright 2024, Elsevier. (D) HRTEM images, (E) charge density difference, (F) planar-averaged charge density difference along the Z-axis of BiOBr/$Bi_4O_5Br_2$. (D-F) Reproduced with permission from[117]. Copyright 2024, American Chemical Society. TEM: Transmission electron microscopy; HRTEM: high-resolution TEM; KTN: $KTa_{0.5}Nb_{0.5}O_3$.

Most photocatalysts, including TiO_2, g-C_3N_4[129,130], and BiOX (X = Cl, Br, I), are constrained ed by rapid recombination of photogenerated electron-hole pairs, which severely limits the number of charge carriers available for N_2 reduction. Despite its suitable band structure and excellent chemical stability, which make $Bi_4O_5Br_2$ promising for photocatalytic nitrogen fixation, the single-component system still suffers from fast charge recombination. To overcome this limitation, Wang *et al.*[117] constructed a direct Z-scheme heterojunction between BiOBr and $Bi_4O_5Br_2$ via a one-step solvothermal method. HRTEM images showed continuous and well-aligned lattice fringes at the BiOBr/$Bi_4O_5Br_2$ interface, confirming a high degree of lattice matching, as shown in Figure 8D. These structural features help reduce interfacial charge transfer resistance and provide a foundation for efficient cross-interface migration of photogenerated charge carriers. Theoretical calculations indicated that electrons predominantly migrate from $Bi_4O_5Br_2$ to BiOBr, resulting in a pronounced charge-density difference at the interface, as shown in Figure 8E. This clearly demonstrates directional electron transfer across the heterojunction. Quantitative charge density analysis along the Z-axis further confirmed electron enrichment on the BiOBr side, as shown in Figure 8F. The BiOBr region displayed increased electron density, while the Bi4O5Br2 area showed a decrease, aligning with the qualitative profile. These findings collectively confirm the direction of electron transfer and the spatial distribution of accumulated electrons. Within the constructed BiOBr/$Bi_4O_5Br_2$ Z-scheme heterojunction, electrons migrate from $Bi_4O_5Br_2$ to BiOBr, whereas holes remain in the valence band of $Bi_4O_5Br_2$. This mechanism promotes the spatial separation of photogenerated electron-hole pairs and effectively inhibits their rapid recombination within individual regions.

In summary, Z-scheme heterojunctions overcome the redox potential loss of Type-II systems by enabling selective recombination of less active carriers, thereby preserving strong reduction and oxidation abilities. Interface engineering - such as conductive bridges, chemical bonding, or noble-metal mediators - is essential to direct the desired charge-transfer pathway and enhance nitrogen-fixation selectivity.

Table 3. Bi-based S-scheme heterojunction for N_2 reduction to NH_3

Photocatalyst	Light source	Reaction solution	Performance ($\mu mol \cdot g^{-1} \cdot h^{-1}$)	Catalyst loading (mg)	Reaction volume (mL)	Ref.
$MoS_2/In\text{-}Bi_2MoO_6$	300 W Xe lamp	H_2O	90	100	100	[44]
$Ti\text{-}BiOBr/TiO_2$	300 W Xe lamp	H_2O	231	100	100	[47]
BiOBr/BiSBr	300 W Xe lamp	H_2O	116.3	20	50	[61]
Bi_2S_3@PCN	300 W Xe lamp	H_2O	228	20	50	[95]
Bi_2S_3/Bi_2MoO_6	300 W Xe lamp	H_2O	126	100	100	[131]
$Bi_2Sn_2O_7$/BiOBr	300 W Xe lamp	H_2O	459.04	50	100	[132]
$Cs_3Bi_2Br_9$/BiOBr	300 W Xe lamp	$(CH_3)_2CHOH/H_2O$	130	5	0.4	[133]
$Cs_3Mo_xSb_yBr_9/BiVO_4$	300 W Xe lamp	$(CH_3)_2CHOH/H_2O$	300 ± 5	3	0.4	[134]
$NaNbO_3/Bi_2O_2CO_3$	300 W Xe lamp	CH_3OH/H_2O	453.1	100	200	[135]
$g\text{-}C_3N_4/Bi_4O_5Br_2$	400 W metal halide lamp	H_2O	151.9	50	-	[136]
$BiSI/TiO_2$ QDs/TiO_{2-x}	500 W Xe lamp	H_2O	6,968	40	40	[137]
$Bi_2O_2CO_3/g\text{-}C_3N_4/SrTiO_3$	300 W Xe lamp	CH_3OH/H_2O	2,173.11	30	100	[138]
$Bi_2Sn_2O_7/Bi_2MoO_6$	300 W Xe lamp	H_2O	275.67	-	50	[139]

S-type heterojunction

The S-type heterojunction is a semiconductor heterostructure that optimizes the separation and transport of photogenerated charge carriers and is widely used in photocatalysis. Its name comes from the stepped band alignment of two semiconductors, not a literal "S-shape". When in contact, their energy bands form a staggered configuration for directional charge migration[102]. Table 3 presents data on S-type heterojunctions over the past few years.

Lv *et al.*[61] successfully constructed an S-scheme BiOBr/BiSBr (BOB/BSB) heterojunction featuring a strongly coupled interface with atomic layer bonding (ALB) via an *in-situ* anion exchange strategy. The interface is characterized by a shared Bi atomic layer and O-Bi-S covalent bonds, which significantly enhance interfacial binding strength and charge-transport capability, as shown in Figure 9A and B. This interfacial engineering strategy drives S-scheme charge transfer and spatial separation via strong orbital hybridization and a reinforced built-in electric field. Meanwhile, oxygen vacancies are introduced to optimize the Fermi level and surface adsorption behavior. The synergistic effect between the strongly coupled ALB interface and oxygen vacancies improves orbital hybridization, promotes N_2 and H_2O activation, and reduces the Gibbs free energy of the rate-determining step, as shown in Figure 9C. Han *et al.*[138] precisely constructed a $Bi_2O_2CO_3/g\text{-}C_3N_4/SrTiO_3$ (BOC/CN/STO) dual S-scheme heterojunction via a multi-step hydrothermal process. This substantially lowers the reaction energy barrier by strengthening the built-in electric field, achieving intimate interfacial coupling and strong electronic interactions among the three components, as shown in Figure 9D. Benefiting from dual built-in electric fields and a staggered band alignment, this system drives efficient separation and directional transport of photogenerated charge carriers along dual S-scheme pathways, suppressing interfacial charge recombination. Compared with single components and conventional binary heterojunctions, this interfacial engineering strategy prolongs carrier lifetimes, enhances interfacial charge-transfer kinetics, and preserves the materials' strong redox capability, as shown in Figure 9E-G.

Recently, our group designed and fabricated a $MoS_2/In\text{-}Bi_2MoO_6$ heterojunction catalyst through electrostatic self-assembly, resulting in interfacial chemical bonding. Instead of mere physical attachment, the Mo-S bonds formed at the interface serve as an "electron bridge" connecting the two materials. This chemical bond

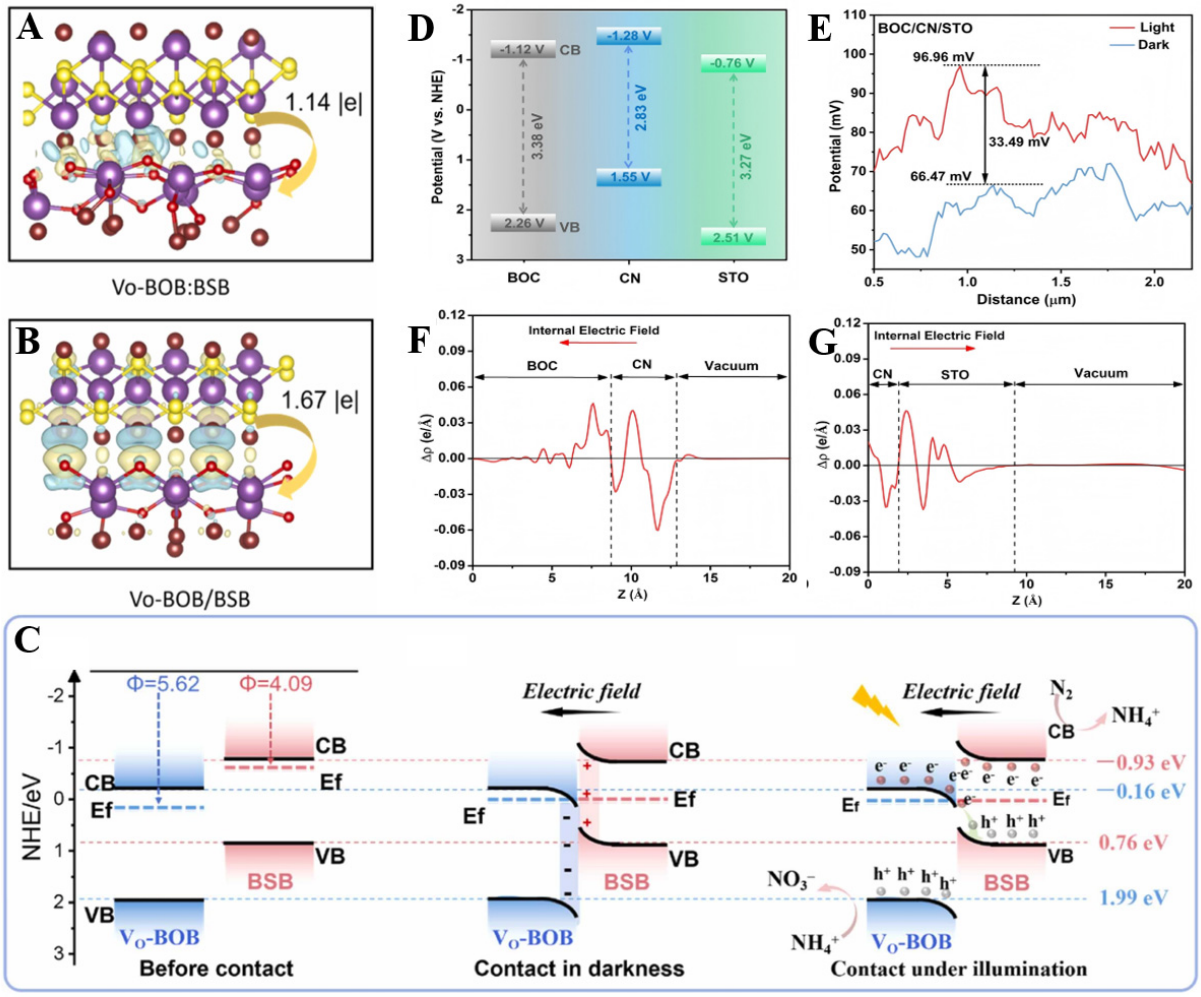

Figure 9. Front-view of the charge difference distribution of physically mixed (A) V_O-BOB:BSB and (B) V_O-BOB/BSB heterojunction. (C) Energy band diagrams before and after V_O-BOB and BSB come into contact, proposed mechanisms for photocatalytic overall N_2 fixation. (A-C) Reproduced with permission from[61]. Copyright 2026, Elsevie; (D) A schematic illustration of band structures for CN, STO, and BOC; (E) Surface potential difference of the BOC/CN/STO under irradiation; Planar-averaged electron density difference Δρ(z) of (F) BOC/CN and (G) CN/STO. Copyright 2026, (D-G) Reproduced with permission from[138]. Wiley-VCH GmbH. BOB: BiOBr; BSB: BiSBr; BOC: $Bi_2O_2CO_3$; CN: g-C_3N_4; STO: $SrTiO_3$; CB: conduction band; VB: valence band; BSB: BiSBr.

, functioning as an electron conduit, removes the interfacial transport barrier. Compared with the Mo-S bond in pure MoS_2[44], the bond length in the heterojunction is elongated by 0.15 Å, which further facilitates electron transfer, as shown in Figure 10A and B. Meanwhile, the work function mismatch between MoS_2 and In-Bi_2MoO_6 induces an interfacial potential difference, resulting in a built-in electric field that directionally drives the migration of photogenerated carriers, thereby promoting electron transfer from In-Bi_2MoO_6 to MoS_2, as shown in Figure 10C. Thus, the separation of charge carriers is addressed from a thermodynamic perspective, which aligns with the fundamental principles of negative charge carriers to achieve the spontaneous assembly of the two materials, thereby constructing an In_2O_3/Bi_2MoO_6 heterojunction[58]. At the interface, In-O-Mo chemical bonds form, serving as an "electron bridge" to remove the physical potential barrier, in line with the fundamental principle of interfacial potential regulation in heterojunction systems. Recently, we employed the electrostatic attraction between positively charged Bi_2MoO_6 and the gap to achieve atomic-level intimate contact between the components, as shown in Figure 10D-F. This facilitates electron transfer from In_2O_3 to Bi_2MoO_6 and establishes a continuous pathway for charge transport. The formation of In-O-Mo bonds create a significant number of oxygen vacancies, which enhance nitrogen adsorption and activation, providing more active sites for photocatalytic nitrogen fixation.

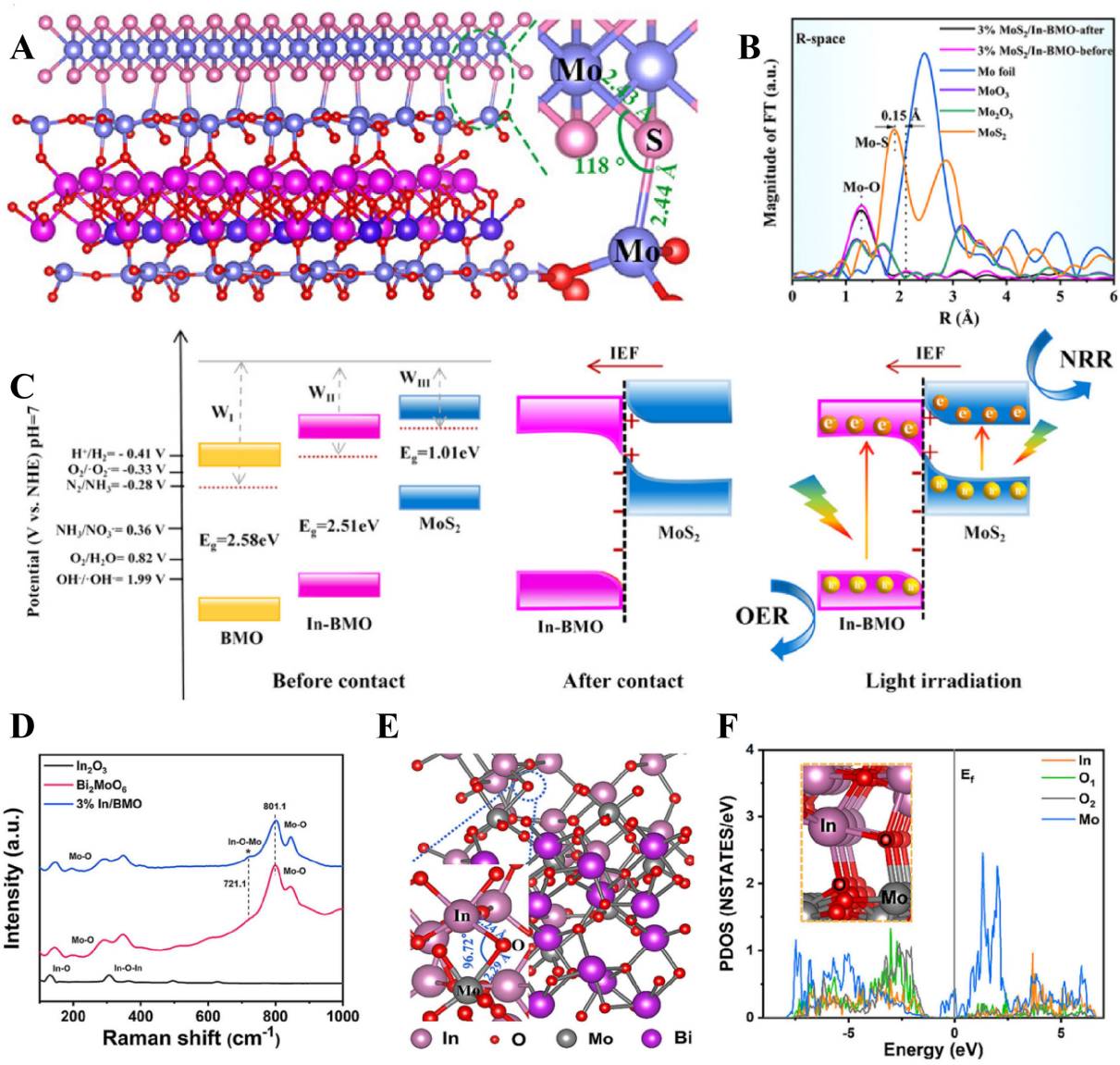

Figure 10. (A) Formation of interfical chemical-bond at MoS_2 and In-Bi_2MoO_6 interface. (B) Mo extended X-xay absorption fine structure spectra shown in the k^3 weighted R-space of 3% MoS_2/In-Bi_2MoO_6. (C) S-scheme photogenerated carrier transfer pathway mechanism. (A-C) Reproduced with permission from[44]. Copyright 2024, American Chemical Societ; (D) Raman spectra of as-prepared samples, and the (E) optimized molecular structure model of 3% In/Bi_2MoO_6. (F) Projection density-of-states of various atoms involved in bonding at the Bi_2MoO_6/In_2O_3 interface. (D-F) Reproduced with permission from[58]. Copyright 2024, Elsevier. NRR: Nitrogen reduction reaction; OER: oxygen evolution reaction; BMO: Bi_2MoO_6; IEF: built-in electric field.

More recently, Ren *et al.*[133] fabricated an S-scheme $Cs_3Bi_2Br_9$/BiOBr heterojunction by growing $Cs_3Bi_2Br_9$ nanocrystals *in situ* on BiOBr hollow nanotubes. This *in situ* transformation strategy enables the formation of intimate interfacial contact within the heterojunction. The interface between $Cs_3Bi_2Br_9$ and BiOBr exhibits a smooth transition without discernible gaps, confirming that the *in situ* approach achieves atomic-level interfacial intimacy and provides an uninterrupted pathway for charge transfer, as shown in Figure 11A. A strong, homogeneous surface photovoltage signal is observed on the sample surface, indicating efficient separation and surface accumulation of photogenerated charge carriers, as shown in Figure 11B and C. Liu *et al.*[134] employed an anti-solvent induction strategy to enable the *in-situ* growth of $Cs_3Mo_xSb_yBr_9$ nanocrystals on $BiVO_4$ nanosheets, thereby forming a tightly connected heterojunction interface. Lattice overlap between the two materials is observed at the interface, without discernible defects or gaps, ensuring efficient charge transport. By varying the amount of $MoBr_4$ added, a series of $Cs_3Mo_xSb_yBr_9$/$BiVO_4$ heterojunctions with

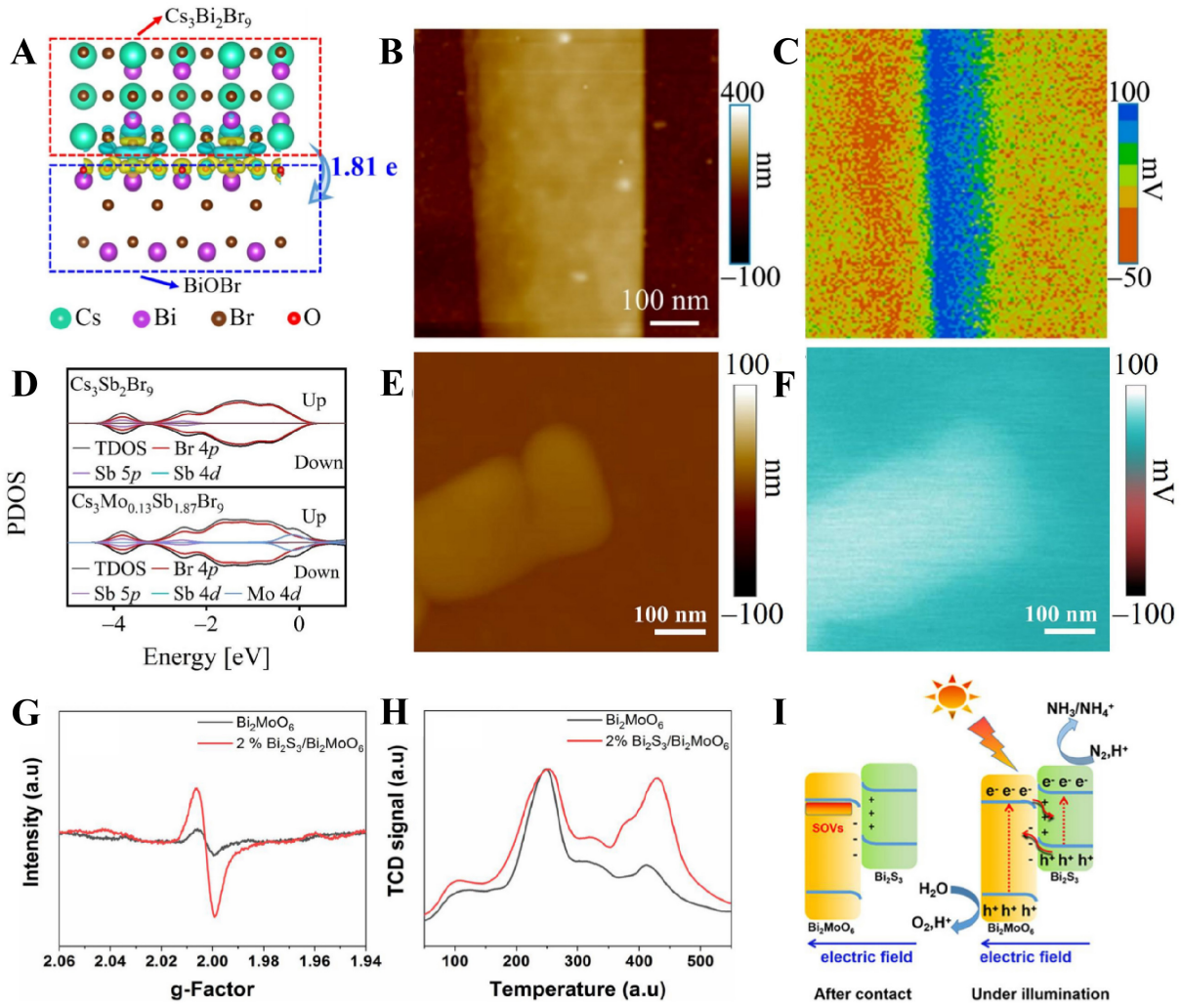

Figure 11. (A) Charge density difference of the $Cs_3Bi_2Br_9$/BiOBr heterojunction. Atomic force microscope (AFM) height images of (B) $Cs_3Bi_2Br_9$/BiOBr. SPV images of (C) $Cs_3Bi_2Br_9$/BiOBr under illumination. (A-C) Reproduced with permission from[133]. Copyright 2024, Elsevier; (D) PDOS configurations of $Cs_3Sb_2Br_9$ and $Cs_3Mo_{0.13}Sb_{1.87}Br_9$. AFM height images of (E) $Cs_3Mo_{0.13}Sb_{1.87}Br_9$/$BiVO_4$. SPV images of (F) $Cs_3Mo_{0.13}Sb_{1.87}Br_9$/$BiVO_4$ under illumination. (D-F) Reproduced with permission from[134]. Copyright 2024, Elsevier; (G) Electron spin resonance spectra, (H) Nitroge temperature-programmed desorption profiles of the catalyst of Bi_2MoO_6 and 2% Bi_2S_3/Bi_2MoO_6. (I) Photocatalytic mechanisms of Bi_2S_3/OV-Bi_2MoO_6. (G-I) Reproduced with permission from[131]. Copyright 2022, Elsevier. PDOS: Partial density of states; SPV: surface photovoltage.

different Mo doping levels was synthesized to optimize the interfacial properties. Upon Mo functionalization, the d-band center of $Cs_3Mo_xSb_yBr_9$ is upshifted toward the Fermi level (from -29.43 eV to -4.31 eV), leading to enhanced N_2 binding and promoted activation of the N≡N bond, as shown in Figure 11D-F.

Recently, our group fabricated a Bi_2S_3/OV-Bi_2MoO_6 heterojunction via an *in-situ* anion-exchange method[131], where Bi_2S_3 nanoparticles were uniformly anchored on the surface of Bi_2MoO_6 without observable physical gaps at the interface, achieving intimate interfacial contact. The strong interaction between Bi_2S_3 and Bi_2MoO_6 during interface formation leads to the reduction of Mo^{6+} to Mo^{5+}, accompanied by the generation of abundant OVs, as shown in Figure 11G. These OVs, together with Bi_2S3, form dual active sites, while the intimate interfacial contact and the introduction of oxygen vacancies synergistically promote N_2 activation, as shown in Figure 11H. Meanwhile, an S-scheme charge transfer pathway enhances the utilization efficiency of photogenerated carriers. Consequently, both the NRR and oxygen evolution reaction (OER) are simultaneously enhanced, as shown in Figure 11I.

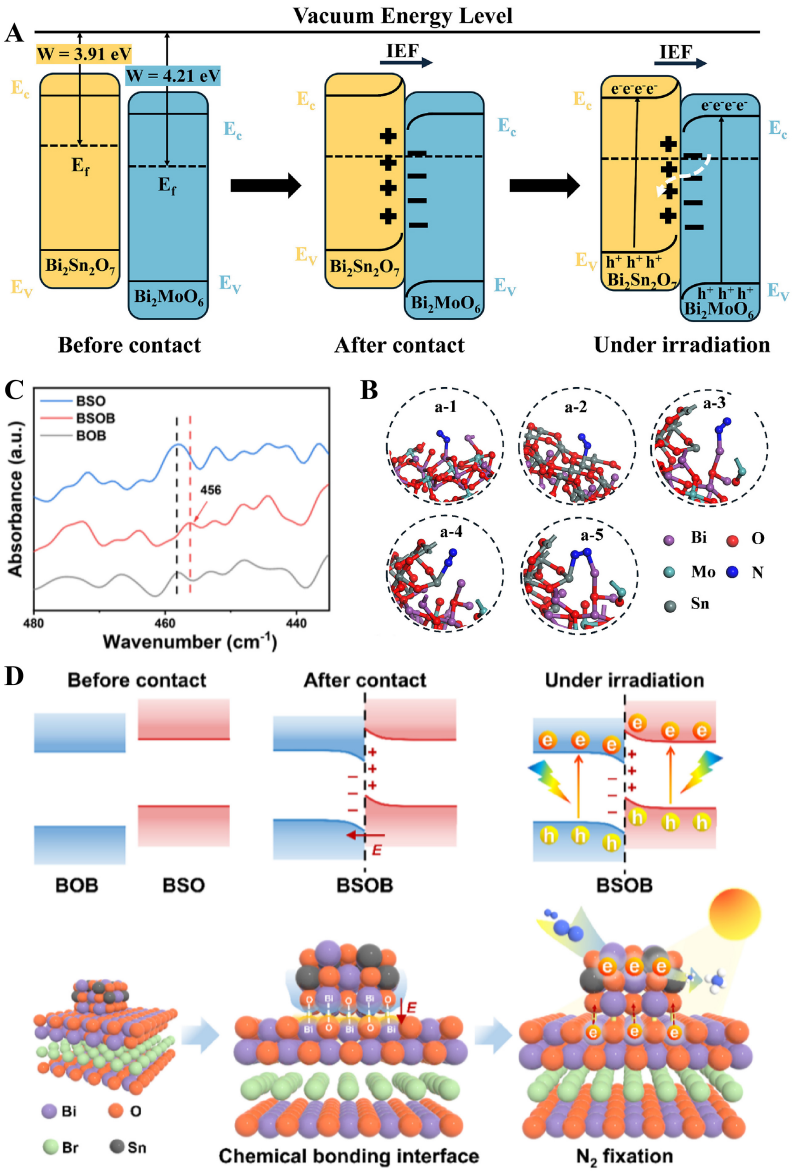

Figure 12. (A) Diagram illustrating the S-scheme charge transfer within the $Bi_2Sn_2O_7/Bi_2MoO_6$ heterojunction. (B) Five possible adsorption configurations of the N_2 molecule on the Bi_2MoO_6 plane, $Bi_2Sn_2O_7$ plane, and $Bi_2Sn_2O_7/Bi_2MoO_6$. (A and B) Reproduced with permission from[139]. Copyright 2026, Elsevier; DMPO spin-trapping Electron Spin Resonance (ESR) spectra of as-prepared samples detected in (C) methanol. (D) The inferred electronic structure model and the mechanism of photocatalytic nitrogen fixation. (C and D) Reproduced with permission from[132]. Copyright 2023, Elsevier. BOB: BiOBr; BSO: $Bi_2Sn_2O_7$; BSOB: $Bi_2Sn_2O_7$; IEF: built-in electric field; DMPO: projected density of states.

Li *et al.*[139] constructed a chemically bonded $Bi_2Sn_2O_7/Bi_2MoO_6$ S-scheme heterojunction. By leveraging the built-in electric field and band bending, they achieved efficient spatial separation of photogenerated charge carriers while preserving strongly reductive electrons and strongly oxidative holes, effectively addressing the key issues of severe carrier recombination and inadequate redox capability in traditional heterojunctions, as shown in Figure 12A. Moreover, the chemically bonded interface induces the formation of asymmetric Bi-Sn dual-atom active sites, enabling side-on adsorption and efficient activation of N_2, thereby significantly reducing the energy barrier for the nitrogen reduction reaction. This enables synergistic regulation of interfacial structure, charge transport, and N_2 activation at the atomic level, ultimately substantially enhancing the photocatalytic nitrogen fixation performance, as shown in Figure 12B.

Zhang *et al.*[132] demonstrated the formation of a heterojunction between $Bi_2Sn_2O_7$ (BSO) and BiOBr (BOB), in which the defective sites (unsaturated Bi and O atoms) on the heterojunction surface interact to create new Bi-O covalent bonds, thereby tightly connecting the two materials, as shown in Figure 12C. This chemically bonded interface, as opposed to mere physical adsorption, establishes a "rigid linkage" that prevents interfacial detachment or charge-transfer blockage. Under illumination, electrons from the CB of BOB and holes from the VB of BSO recombine rapidly via the Bi-O bonds (deactivating less reactive carriers). In contrast, the highly reductive electrons in the CB of BSO and the oxidative holes in the VB of BOB are preserved. The Bi and Sn atoms surrounding oxygen vacancies on the BSO surface provide active sites for N_2 adsorption, as shown in Figure 12D. The accumulated electrons are efficiently transferred through the Bi-O bonds to the adsorbed N_2 molecules, weakening the N≡N bond and lowering the energy barrier to nitrogen reduction.

In summary, S-scheme heterojunctions effectively address key challenges in photocatalytic nitrogen fixation, such as low charge separation efficiency and the difficult activation of N_2, by leveraging stepped band alignment, a built-in electric field, and selective carrier recombination. Further advances in interfacial engineering, active site design, and system optimization may further promote their practical application in green ammonia synthesis.

Other heterojunction

Beyond the heterojunctions previously discussed, other heterojunctions, such as ohmic heterojunctions, have also been explored. For instance, Zheng *et al.*[140] prepared a structurally aligned 2D-2D ohmic heterojunction by epitaxially growing a two-dimensional bismuth layer on BiOBr nanosheets via *in situ* annealing, as shown in Figure 13A. This process formed a Schottky-barrier-free ohmic contact interface, eliminating the energy barrier to electron transfer and establishing a nearly impedance-free charge-transport channel, as shown in Figure 13B and C. Simultaneously, high-density OVs were introduced at the BiOBr interface during annealing, as shown in Figure 13D. The formed Bi-BiOBr coordination bonds at the interface alter the chemical environment of surrounding atoms, further optimizing the electronic structure for N_2 adsorption, weakening the N≡N bond energy, and promoting the activation and dissociation of N_2, as shown in Figure 13E. *In situ* Fourier transform infrared Spectroscopy (FTIR) spectroscopy confirmed that the Bi/BiOBr interface significantly enhances the chemical adsorption of N_2, and the adsorbed N_2 can directly participate in the subsequent reactions, as shown in Figure 13F and G.

CONCLUSIONS AND PERSPECTIVES

This review delineates recent developments in photocatalytic nitrogen fixation utilizing bismuth-based heterojunctions. It commences with an elucidation of the fundamental principles underpinning photocatalytic nitrogen fixation and the primary structural characteristics of Bi-based materials. Subsequently, it offers a comprehensive discussion of various heterojunction engineering strategies: Type-II heterojunctions facilitate charge separation; Z-scheme heterojunctions augment redox capability; and S-scheme heterojunctions promote efficient carrier migration. The review also assesses different ammonia detection methodologies. Despite notable advancements in nitrogen reduction employing bismuth-based heterojunction photocatalysts, several challenges persist; future research should aim to overcome current limitations to fully utilize the distinctive advantages of these heterojunctions. Additionally, subsequent investigations should employ reliable detection techniques and explore coupled reaction systems. Continued innovation is imperative for the realization of practical, solar-driven ammonia synthesis. By delineating these directions, the review aspires to influence sustainable nitrogen fixation strategies, guide future scholarly endeavors, and enhance both academic impact and commercial viability.

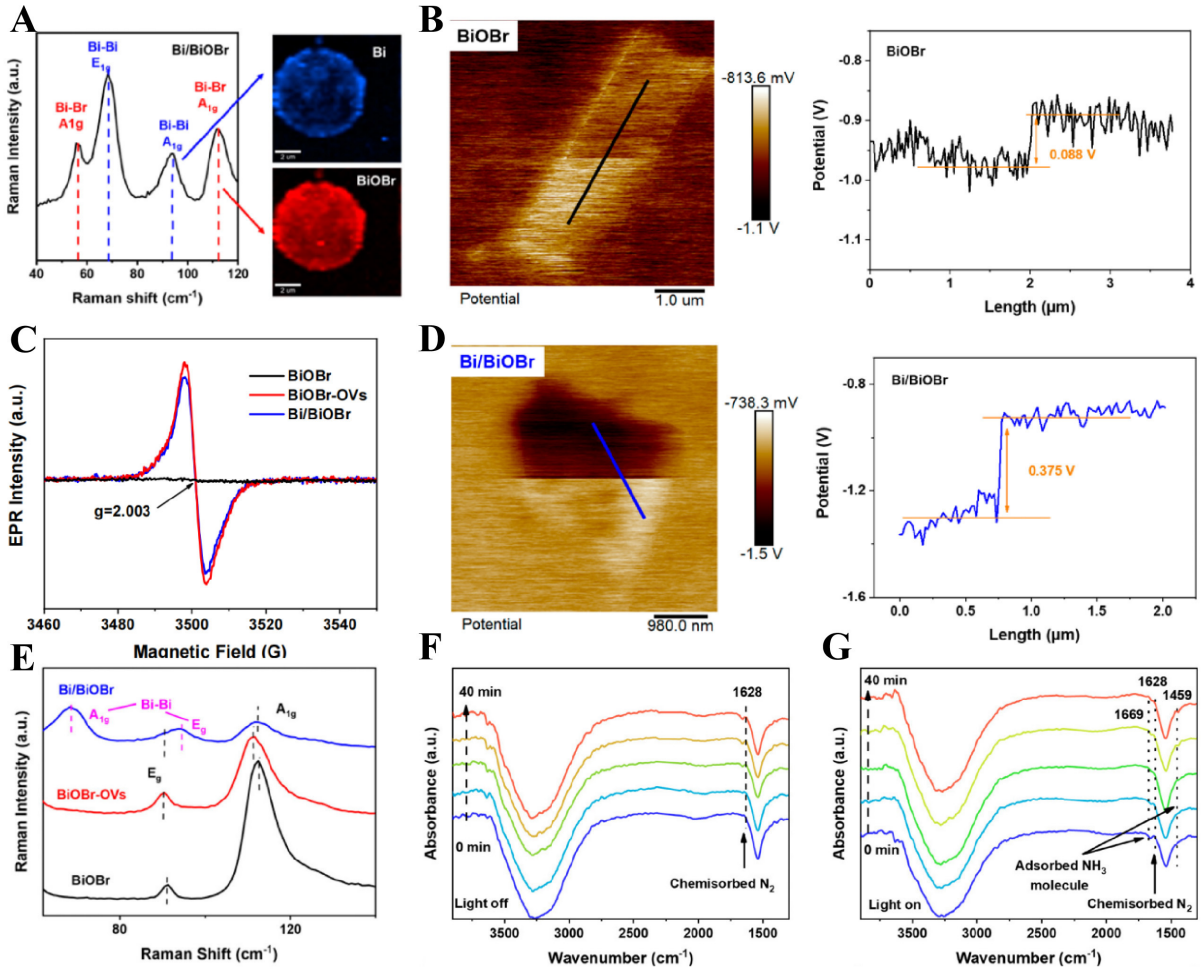

Figure 13. (A) Raman mapping images of the BiOBr, BiOBr-OVs, and Bi/BiOBr. Kelvin probe force microscopy (KPFM) images and the potential change spectrum of the lines: (B) BiOBr, (C) Bi/BiOBr. (D) EPR spectra and (E) Raman spectra of BiOBr, BiOBr-OVs, and Bi/BiOBr. Characterization of photocatalytic nitrogen fixation: *in situ* FTIR spectra with (F) light off and (G) light on. (A-G) Reproduced with permission from[140]. Copyright 2024, American Chemical Society. EPR: Electron paramagnetic resonance; FTIR: fourier transform infrared spectroscopy; OVs: oxygen vacancies.

Engineering intimate interfaces for superior photocatalysis

To achieve higher photocatalytic performance, constructing a more intimate heterojunction interface is a key strategy. Close interfacial contact can significantly enhance the efficient separation and migration of photogenerated charge carriers, thereby effectively suppressing electron-hole pair recombination. The interfacial contact area can be enhanced through the following approaches. The first approach involves constructing a core-shell heterojunction. In this design, one semiconductor material serves as the "core", tightly encapsulated by a complete "shell" formed from another material. This three-dimensional omnidirectional contact creates a substantial interfacial contact area and establishes clear, continuous pathways for charge transfer between the two materials. The second approach is the *in-situ* growth synthesis method. Unlike traditional physical mixing, this method involves the direct chemical "growth" of a second material on a substrate, resulting in atomic- or molecular-scale interfacial bonding. These synthesis methods can ensure very tight, uniform heterojunction interfaces, reduce interfacial defects, and often achieve lattice matching, providing an optimal pathway for charge transfer. The third approach is surface ligand passivation. In this method, specific chemical molecules bind to the surface atoms of nanomaterials (such as quantum dots, metal nanoparticles, or semiconductor thin films), saturating the dangling bonds on the surface. This eliminates or neutralizes surface defect states and steers the surface chemical activity toward a

direction more favorable for the target photocatalytic reaction. The fourth method is atomic layer deposition (ALD), a thin-film fabrication technique based on self-limiting surface chemical reactions. In a typical ALD process, two or more gaseous precursors are alternately pulsed into the reaction chamber. Each precursor chemisorbs onto the substrate surface and reacts until saturation, after which an inert gas purges away the excess precursor. One complete cycle - precursor A pulse, purge, precursor B pulse, purge - grows a single atomic layer. Thus, the film thickness can be controlled with atomic-scale precision simply by adjusting the number of cycles. This precise control provided by ALD facilitates the balance between light absorption and charge separation. Furthermore, by alternating between various precursors, it is possible to produce multilayered, doped, or compositionally graded films. In photocatalytic applications, exposed surface defects often serve as catalysts for side reactions. Post-ALD deposition, the surface chemical activity is diminished, leading to improved selectivity toward the desired reaction. The fifth technique involves electrochemical interface reconstruction. By applying a controlled electrochemical potential during or subsequent to catalyst synthesis, the surface composition, oxidation state, and atomic configuration of bismuth-based photocatalysts can be dynamically adjusted. This *in situ* or *ex situ* reconstruction enables the formation of new active interfaces, the removal of unstable surface species, and the optimization of contact between different components, thereby enhancing charge transfer and reaction kinetics. Electrochemical reconstruction represents a versatile and tunable approach to generate intimate heterointerfaces that are challenging to achieve through conventional chemical synthesis.

Converging materials and synthetic biology for solar nitrogen fixation

Developing innovative photocatalytic N_2 fixation systems through the integration of materials science and synthetic biology. For example, artificial bio-inspired systems can be engineered by coupling bismuth-based light-harvesting units with molecular mimics of the nitrogenase active site, thereby facilitating the directional transfer of photogenerated electrons to the catalytic center and emulating the high selectivity of enzymatic processes. Additionally, bio-inorganic hybrid systems may be constructed, such as assembling bismuth-based catalysts on the surface of engineered microorganisms. This integrated approach enables solar energy to synergistically enhance endogenous nitrogen fixation metabolism, supporting efficient solar-driven biosynthesis.

Designing integrated systems for multi-energy N_2 fixation

The development of photo-electro-thermal coupled catalytic systems presents a promising approach to overcome the efficiency limitations of single-mode photocatalytic nitrogen fixation. By applying an electric field, the directional separation and migration of photogenerated carriers can be effectively driven, charge recombination can be suppressed, and the catalyst surface potential can be modulated to optimize N_2 adsorption and activation barriers. When combined with mild heating at 50-100 °C, the adsorption and diffusion of N_2 molecules on the catalyst surface are enhanced, and the conversion kinetics of key intermediates are accelerated, addressing the sluggish reaction rates typically observed under ambient conditions. This synergistic multi-field strategy not only increases the ammonia synthesis rate but also suppresses competing HER through precise energy barrier modulation, thus improving process selectivity. Future research should aim to design integrated catalyst-reactor systems tailored for multi-field operation to enable efficient coupling and conversion of optical, electrical, and thermal energy inputs.

Coupling nitrogen fixation with hole-driven catalysis

The photocatalytic NRR employs photogenerated electrons to reduce N_2 molecules. In conventional processes, sacrificial hole scavengers are commonly used to consume photogenerated holes. However, given their potent oxidizing ability, these holes can be strategically used to drive catalytic oxidation reactions for the synthesis of higher-value chemicals. Examples include organic transformations, such as the conversion of benzyl alcohol to benzaldehyde and 5-hydroxymethylfurfural (HMF) to 2,5-furandicarboxylic acid (FDCA),

as well as pollutant degradation. Harnessing photogenerated holes in this way promises to broaden the application potential of photocatalytic technology significantly.

Standardization and normalization methods for evaluating photocatalytic nitrogen fixation performance

The ammonia yield rates reported in different studies are often difficult to compare directly, owing to significant variations in reactor configuration, light source type and intensity, catalyst loading, reaction volume, illuminated area-to-reaction volume ratio, and product detection methods. Therefore, establishing a standardized approach to reporting performance is an urgent need to promote the healthy development of this field. In photocatalytic nitrogen fixation studies, reactors with identical configuration and volume should be used whenever possible, and the light intensity and wavelength should be described in detail to facilitate comparison. Meanwhile, ion chromatography should be preferentially adopted as the detection method due to its higher accuracy.

Reactor design and scalable synthesis

To facilitate the transition toward practical application, advancements in both reactor engineering and scalable fabrication techniques are indispensable. In reactor design, research should prioritize the development of efficient systems, such as continuous-flow fixed-bed or membrane reactors. Structural optimization efforts should aim to enhance light distribution and improve gas-liquid-solid triphase mass transfer, thereby increasing light utilization efficiency, ammonia production rate, and operational stability. Concerning scalable fabrication, strategies must strike a balance between performance and cost, with an emphasis on environmentally sustainable and scalable synthesis routes. This includes reducing reliance on precious-metal cocatalysts and investigating cost-effective alternatives based on transition metals or non-metals. A systematic assessment of scalability from gram-scale laboratory synthesis to kilogram- and ton-scale industrial production is essential, as it addresses process stability, energy consumption, and environmental impact. For instance, a continuous-flow fixed-bed reactor immobilizes the photocatalyst as a thin film or packed bed within a transparent reaction channel. Gaseous nitrogen and liquid water flow continuously over the catalyst surface, where the photocatalytic reaction proceeds and produces an ammonia-containing effluent stream. Unlike conventional batch reactors, the fixed-bed configuration enables a "reaction-and-outflow" operational mode, eliminating the laborious post-reaction separation of the catalyst from the reaction medium. Moreover, because the catalyst is fixed to the channel surface, the light-scattering and shielding effects typically caused by catalyst agglomeration in conventional suspension systems are avoided, thereby enhancing photon utilization efficiency.

DECLARATIONS

Authors' contributions

Conceptualization, resources, writing-review & editing: Zhang, D.; Guo, L.; Wang, D.
Conceptualization, data curation, investigation, formal analysis: Li, Z.
Data curation: Yang, C.
Data curation, investigation: Wang, T.

Availability of data and materials

Not applicable.

AI and AI-assisted tools statement

Not applicable.

Financial support and sponsorship

This work was financially supported by the National Natural Science Foundation of China (No. 22568049), the Science and Technology Planning Project of Yan'an City (No. 2024-CYL-030), and the Yan'an University Graduate Student Scientific Research Innovation Program Project (No. YKY2025066).

Conflicts of interest

All authors declared that there are no conflicts of interest.

Ethical approval and consent to participate

Not applicable.

Consent for publication

Not applicable.

REFERENCES

1. Majumder, M.; Saini, H.; Dědek, I.; et al. Rational design of graphene derivatives for electrochemical reduction of nitrogen to ammonia. *ACS. Nano.* **2021**, *15*, 17275-98. DOI
2. Liu, Y.; Fernández, C. A.; Varanasi, S. A.; Bui, N. N.; Song, L.; Hatzell, M. C. Prospects for aerobic photocatalytic nitrogen fixation. *ACS. Energy. Lett.* **2021**, *7*, 24-9. DOI
3. Li, H.; Wang, J.; Ruan, Z.; et al. Electron transfer bridge inducing polarization of nitrogen molecules for enhanced photocatalytic nitrogen fixation. *Mater. Horiz.* **2023**, *10*, 5053-9. DOI
4. Boretti, A. Advancing ammonia synthesis: pathways toward decarbonization and sustainability. *Chem. Eng. Res. Des.* **2025**, *217*, 235-51. DOI
5. Wang, T.; Zhai, R.; Liu, Z.; Liu, S.; Cheng, Y.; Zhang, J. Electron donation of violet phosphorene nanosheets to sustain the oxygen vacancies of BiOBr for excellent photocatalytic nitrogen fixation. *J. Mater. Chem. A.* **2025**, *13*, 13551-9. DOI
6. Wang, X. H.; Wu, B.; Zhu, Y.; et al. Design refinement of catalytic system for scale-up mild nitrogen photo-fixation. *Nano. Micro. Lett.* **2025**, *17*, 182. DOI PubMed PMC
7. Ge, X.; Zheng, X.; Zhou, T.; et al. Engineering spin state of atomic iron centers for high-performance photocatalytic nitrogen fixation. *Angew. Chem. Int. Ed.* **2025**, *64*, e202506470. DOI
8. Chen, T. Y.; Ying, Y. R.; Wu, J.; Liu, X. H.; Huang, H. Fe-N_4-anchored carbon layer patched TiO_2 cavities to construct an "in-lattice heterojunction" for enhanced photocatalytic nitrogen reduction reactions. *Angew. Chem. Int. Ed.* **2025**, *64*, e202509705. DOI
9. Qu, J.; Zhu, Z.; Xu, X.; et al. Single-atom Cu anchoring on heterocyclic ring of metal-organic frameworks for photocatalytic nitrogen fixation. *Small. Methods.* **2025**, *10*, 2500493. DOI
10. Liu, C.; Liu, Y.; Xu, G.; Wang, T. Associative-distal mechanism of the haber-bosch process on a ferrierite catalyst with spatially isolated dual molybdenum sites. *J. Phys. Chem. C.* **2024**, *128*, 6711-8. DOI
11. Liu, C.; Xu, G.; Wang, T. Theoretical approach toward a mild condition haber-bosch process on the zeolite catalyst with confined dual active sites. *JACS. Au.* **2023**, *3*, 3374-80. DOI
12. Wang, J.; Tang, Y.; Yang, Q.; et al. Enhanced photocatalytic nitrogen fixation via Pt-induced active hydrogen supply over Pt@NM-101(Fe). *Appl. Catal. B. Environ. Energy.* **2025**, *373*, 125364. DOI
13. Xia, M.; Gong, X.; Teng, W.; et al. Nanopit-mediated electron pooling effect for efficient piezo-photocatalytic N_2 fixation in pure water. *Appl. Catal. B. Environ. Energy.* **2026**, *380*, 125756. DOI
14. Schrauzer, G. N.; Guth, T. D. Photolysis of water and photoreduction of nitrogen on titanium dioxide. *J. Am. Chem. Soc.* **2002**, *99*, 7189-93. DOI
15. Mao, S.; He, R.; Song, S. S-scheme heterojunction with ultrafast interfacial electron transfer for artificial photosynthesis. *Chin. J. Catal.* **2024**, *64*, 1-3. DOI
16. Hao, P.; Chen, Z.; Yan, Y.; Shi, W.; Guo, F. Recent advances, application and prospect in g-C_3N_4-based S-scheme heterojunction photocatalysts. *Sep. Purif. Technol.* **2024**, *330*, 125302. DOI
17. Li, J.; Zhang, C.; Bao, T.; et al. Dual near-infrared-response S-scheme heterojunction with asymmetric adsorption sites for enhanced nitrogen photoreduction. *Adv. Mater.* **2024**, *37*, 2416210. DOI
18. Wang, X.; Li, Y.; Feng, L.; Yang, Y.; Zheng, X. Construction of BiOBr/hydrophobic carbon cloth heterojunction with internal electric field for enhanced photocatalytic nitrogen fixation. *Small* **2025**, *21*, e03853. DOI
19. Zhang, Y.; Wang, Y.; Wu, X.; et al. Photocorrosion of metal sulfides: mechanism, characterization, anti-photocorrosion strategies and solar catalysis applications. *Coord. Chem. Rev.* **2025**, *545*, 217021. DOI
20. Xia, P.; Pan, X.; Jiang, S.; et al. Designing a redox heterojunction for photocatalytic "overall nitrogen fixation" under mild conditions. *Adv. Mater.* **2022**, *34*, 2200563. DOI

21. Xiong, L.; Hu, Y.; Yang, Y.; et al. Electron pump strengthened facet engineering: organic half-metallic $C(CN)_3$ enclosed (100) facet exposed WO_3 for efficient and selective photocatalytic nitrogen fixation. *Appl. Catal. B. Environ.* **2022**, *317*, 121660. DOI
22. Wang, C.; Wang, S.; Ping, Y.; et al. Ru@MIL-125/MnOx metal-organic-framework-based cocatalysts for photocatalytic nitrogen fixation. *Appl. Catal. B. Environ. Energy.* **2024**, *347*, 123781. DOI
23. Hu, J.; An, K.; Ren, Y.; et al. Plasmonic MoO_{3-x}/Ag Photocatalyst for the fixation of N_2 from air with the solar energy conversion efficiency reaching over 0.28%. *Adv. Mater.* **2025**, *37*, e09652. DOI
24. Cheng, M.; Li, H.; Wu, Z.; Yu, Z.; Tao, X.; Huang, L. Synergistic effects of CQDs and oxygen vacancies on CeO_2 photocatalyst for efficient photocatalytic nitrogen fixation. *Sep. Purif. Technol.* **2025**, *354*, 129299. DOI
25. Wang, F.; Yang, W.; Ding, Q.; et al. Chiral Au@CeO_2 helical nanorods with spatially separated structures for polarization-dependent N_2 photofixation. *Angew. Chem. Int. Ed.* **2024**, *64*, e202415031. DOI
26. Zhang, H.; Bao, L.; Pan, Y.; Ge, J. Doping carbon dots on etched CeO_2-based bimetallic hydroxides for improved photocatalytic ammonia production. *Solar. Energy.* **2023**, *264*, 112002. DOI
27. Lan, M.; Wang, Y.; Dong, X.; et al. Controllable fabrication of sulfur-vacancy-rich Bi_2S_3 nanorods with efficient near-infrared light photocatalytic for nitrogen fixation. *Appl. Surf. Sci.* **2022**, *591*, 153205. DOI
28. Chen, L.; Dai, X.; Li, X.; et al. A novel Bi_2S_3/$KTa_{0.75}Nb_{0.25}O_3$ nanocomposite with high efficiency for photocatalytic and piezocatalytic N_2 fixation. *J. Mater. Chem. A.* **2021**, *9*, 13344-54. DOI
29. Lan, M.; Dong, X.; Zheng, N.; Zhang, X.; Wang, Y.; Zhang, X. In-situ construction of novel sulfur-vacancy-rich Bi/Bi_2S_3/SnS_2 Z-scheme heterostructure photocatalysts for efficient Cr(VI) reduction and nitrogen fixation. *J. Mater. Sci. Technol.* **2023**, *167*, 237-47. DOI
30. Bi, Y.; Fang, Y.; Yuan, L.; et al. Chemically bonded schottky junction for efficient N_2 photofixation. *ACS. Catal.* **2024**, *15*, 246-54. DOI
31. Dong, Q.; Li, X.; Sun, J.; et al. Regulating concentration of surface oxygen vacancies in Bi_2MoO_6/Bi-MOF for boosting photocatalytic ammonia synthesis. *J. Catal.* **2024**, *433*, 115489. DOI
32. Ren, G.; Zhao, J.; Zhao, Z.; et al. Defects-induced single-atom anchoring on metal-organic frameworks for high-efficiency photocatalytic nitrogen reduction. *Angew. Chem. Int. Ed.* **2023**, *63*, e202314408. DOI
33. Sun, Y.; Ji, H.; Sun, Y.; et al. Synergistic effect of oxygen vacancy and high porosity of nano MIL-125(Ti) for enhanced photocatalytic nitrogen fixation. *Angew. Chem. Int. Ed.* **2023**, *63*, e202316973. DOI
34. Nguyen, T. T.; Edalati, K. High-entropy oxide with tailored heterogeneous electronic structure as a low-bandgap catalyst for antibiotic photodegradation under visible light. *Appl. Catal. B. Environ. Energy.* **2026**, *382*, 126011. DOI
35. Zhang, S.; Zhao, Y.; Shi, R.; et al. Efficient photocatalytic nitrogen fixation over $Cu^{\delta+}$-modified defective ZnAl-layered double hydroxide nanosheets. *Adv. Energy. Mater.* **2020**, *10*, 1901973. DOI
36. Zhao, Y.; Zhao, Y.; Waterhouse, G. I. N.; et al. Layered-double-hydroxide nanosheets as efficient visible-light-driven photocatalysts for dinitrogen fixation. *Adv. Mater.* **2017**, *29*, 1703828. DOI
37. Chen, J.; Zang, S.; Gao, K.; Zhang, C.; Wang, X.; Liu, H. Efficient photocatalytic nitrogen fixation over novel 2D/2D $Bi_{12}O_{17}Br_2$/ZnCr layered double hydroxide heterojunction. *Appl. Surf. Sci.* **2023**, *639*, 158216. DOI
38. Zhang, Y.; Zhang, J.; Yi, Q.; et al. *In situ* construction of porous β-Bi_2O_3/BiOCOOH heterojunction photocatalysts: enhancing nitrogen fixation activity by the synergistic effect of oxygen vacancies and lattice oxygen. *ACS. Appl. Energy. Mater.* **2022**, *5*, 9503-11. DOI
39. Tan, C.; Ai, L.; Wang, L.; Jia, D.; Guo, N.; Zha, M. Revealing the nature of asymmetric Lewis acid sites by dual-orbital hybridization in Tb-$BiO_{1-x}Cl$/$BiO_{1-x}Cl$ homostructure for superior photocatalytic performance. *Appl. Catal. B. Environ. Energy.* **2025**, *373*, 125336. DOI
40. Liu, C.; Xiang, Y.; Dong, X.; Wang, Y.; Niu, J.; Zheng, N. Modulation of bismuth vacancies on BiOCl surface by tungsten doping for photocatalytic nitrogen reduction. *Sep. Purif. Technol.* **2025**, *361*, 131424. DOI
41. Shen, Z.; Li, F.; Lu, J.; et al. Enhanced N_2 photofixation activity of flower-like BiOCl by in situ Fe(III) doped as an activation center. *J. Colloid. Interface. Sci.* **2021**, *584*, 174-81. DOI
42. Yang, C.; Zhang, Y.; Yue, F.; et al. Co doping regulating electronic structure of Bi_2MoO_6 to construct dual active sites for photocatalytic nitrogen fixation. *Appl. Catal. B. Environ.* **2023**, *338*, 123057. DOI
43. Ma, T.; Yang, C.; Guo, L.; et al. Refining electronic properties of Bi_2MoO_6 by in-doping for boosting overall nitrogen fixation via relay catalysis. *Appl. Catal. B. Environ.* **2023**, *330*, 122643. DOI
44. Ma, T.; Li, R.; Huang, Y.; et al. Interfacial chemical-bonded MoS_2/In-Bi_2MoO_6 heterostructure for enhanced photocatalytic nitrogen-to-ammonia conversion. *ACS. Catal.* **2024**, *14*, 6292-304. DOI
45. Zhang, L.; Zhou, X.; Liu, S.; et al. Two birds, one stone: rational design of Bi-MOF/g-C_3N_4 photocatalyst for effective nitrogen fixation and pollutants degradation. *J. Clean. Prod.* **2023**, *425*, 138912. DOI

46. Wang, Y.; Li, Z.; Zhu, H.; et al. S-scheme homojunction and activate site engineering over TiO_2 for highly efficient photocatalytic nitrogen fixation. *Chem. Eng. J.* **2024**, *484*, 149583. DOI
47. Li, R. Q.; Bian, Y. J.; Yang, C. M.; et al. Electronic structure regulation and built-in electric field synergistically strengthen photocatalytic nitrogen fixation performance on Ti-BiOBr/TiO_2 heterostructure. *Rare. Met.* **2023**, *43*, 1125-38. DOI
48. Shi, K.; Meng, H.; Liu, J.; Ma, S.; Tang, W. Synergistic contact-electro-catalysis and photocatalysis via TiO_2@PTFE composites for efficient N_2 to NH_3 conversion. *Angew. Chem. Int. Ed.* **2025**, *64*, e202515707. DOI
49. Ding, Z.; Li, X.; Kang, C.; et al. Single ru atoms confined into MOF/C_3N_4 for dual improved photocatalytic carbon dioxide reduction and nitrogen fixation. *Chem. Eng. J.* **2023**, *473*, 145256. DOI
50. Jia, B.; Sui, G.; Zhuang, Y.; et al. Platinum single atom anchoring on nano-MOF/tubular carbon nitride enabled nitrogen activation and multiple electron transfer for photocatalytic nitrogen fixation. *J. Colloid. Interface. Sci.* **2025**, *700*, 138410. DOI
51. Zeng, H.; Liu, L.; Zhang, D.; et al. Fe(III)-C_3N_4 hybrids photocatalyst for efficient visible-light driven nitrogen fixation. *Mater. Chem. Phys.* **2021**, *258*, 123830. DOI
52. Zhang, L.; Gu, R.; Zhang, J.; et al. Plasmonic Bi-doped Bi-$Bi_2Sn_2O_7$/Bi-g-C_3N_4 photothermal catalysis for nitrogen fixation. *Green. Chem.* **2025**, *27*, 2138-49. DOI
53. Wang, X.; Gao, R.; Fan, G.; et al. Dual Defects-induced iron single atoms immobilized in metal-organic framework-derived hollow BiOBr microtubes for low-barrier photocatalytic nitrogen reduction. *Angew. Chem. Int. Ed.* **2025**, *64*, e202501297. DOI
54. Dong, X.; Cui, Z.; Shi, X.; et al. Insights into dynamic surface bromide sites in $Bi_4O_5Br_2$ for sustainable N_2 photofixation. *Angew. Chem. Int. Ed.* **2022**, *61*, e202200937. DOI
55. Liu, L.; Liu, J.; Sun, K.; Wan, J.; Fu, F.; Fan, J. Novel phosphorus-doped Bi_2WO_6 monolayer with oxygen vacancies for superior photocatalytic water detoxication and nitrogen fixation performance. *Chem. Eng. J.* **2021**, *411*, 128629. DOI
56. Liu, Z.; Luo, M.; Yuan, S.; et al. Boron-doped graphene quantum dot/bismuth molybdate composite photocatalysts for efficient photocatalytic nitrogen fixation reactions. *J. Colloid. Interface. Sci.* **2023**, *650*, 1301-11. DOI
57. Yang, F.; Su, Y.; Lin, G.; et al. Synergistic effects of Fe/Br co-doped bismuth molybdate for enhanced photocatalytic nitrogen fixation. *Sep. Purif. Technol.* **2025**, *378*, 134552. DOI
58. Huang, X.; Du, R.; Zhang, Y.; et al. Modulating charge oriented accumulation via interfacial chemical-bond on In_2O_3/Bi_2MoO_6 heterostructures for photocatalytic nitrogen fixation. *J. Colloid. Interface. Sci.* **2024**, *664*, 33-44. DOI
59. Shen, R.; Li, N.; Qin, C.; et al. Heteroatom- and bonded Z-scheme channels-modulated ultrafast carrier dynamics and exciton dissociation in covalent triazine frameworks for efficient photocatalytic hydrogen evolution. *Adv. Funct. Mater.* **2023**, *33*, 2301463. DOI
60. Xu, L.; Zhang, Y.; Liu, B.; et al. Strengthening bonding interaction of a $(Co_{0.91}V_{0.09})_3(BTC)_2$ metal-organic framework with $BiVO_4$ photoanodes enabling ultrastable photoelectrochemical water oxidation. *ACS. Nano.* **2025**, *19*, 15863-75. DOI
61. Lv, S.; Li, K.; Zhang, D.; et al. Anion-exchange-induced synthesis of an atomic layer bonding coupled BiOBr/BiSBr heterojunction: a highly efficient S-scheme photocatalyst for overall nitrogen fixation. *Appl. Catal. B. Environ. Energy.* **2026**, *393*, 126790. DOI
62. Wang, X.; Wang, B.; Yin, S.; Xu, M.; Yang, L.; Sun, H. Highly efficient photocatalytic nitrogen fixation on bio-inspired triphase interface with improved diffusion of nitrogen. *J. Clean. Prod.* **2022**, *360*, 132162. DOI
63. Li, X.; Dong, Q.; Wang, J.; et al. Molecular engineering of active fe center in metalloporphyrin coupled with polyoxometalates for efficient photochemical nitrogen fixation: synergistic effect of multiactive sites strengthening metal-N-N* interactions. *Adv. Funct. Mater.* **2025**, *35*, 2424128. DOI
64. Liang, H.; Ye, C.; Wu, Y.; et al. Fe single atom trigger asymmetric In-In polarized site pairs boosting near-infrared N_2 photoreduction. *Mater. Today.* **2025**, *86*, 96-103. DOI
65. Hu, K.; Huang, Z.; Zeng, L.; et al. Recent advances in MOF-based materials for photocatalytic nitrogen fixation. *Eur. J. Inorg. Chem.* **2021**, *2022*, e202100748. DOI
66. Hao, Q.; Liu, C.; Jia, G.; et al. Catalytic reduction of nitrogen to produce ammonia by bismuth-based catalysts: state of the art and future prospects. *Mater. Horiz.* **2020**, *7*, 1014-29. DOI
67. Bo, Y.; Wang, H.; Lin, Y.; et al. Altering hydrogenation pathways in photocatalytic nitrogen fixation by tuning local electronic structure of oxygen vacancy with dopant. *Angew. Chem. Int. Ed.* **2021**, *60*, 16085-92. DOI
68. Zhu, C.; Zhang, L.; Cui, L.; et al. Fe-Bi dual sites regulation of $Bi_2O_{2.33}$ nanosheets to promote photocatalytic nitrogen fixation activity. *J. Colloid. Interface. Sci.* **2024**, *661*, 46-58. DOI
69. Sun, Y.; Ahmadi, Y.; Kim, K.; Lee, J. The use of bismuth-based photocatalysts for the production of ammonia through photocatalytic nitrogen fixation. *Renew. Sustain. Energy. Rev.* **2022**, *170*, 112967. DOI
70. Kim, T.; Kang, M. J.; Kwon, N. H.; et al. Hybridization-driven introduction of anion vacancies to boost the photocatalytic nitrogen fixation functionality of low-lattice-energy nanosheets. *ACS. Nano.* **2025**, *19*, 29798-812. DOI

71. Di, J.; Xia, J.; Li, H.; Guo, S.; Dai, S. Bismuth oxyhalide layered materials for energy and environmental applications. *Nano. Energy.* **2017**, *41*, 172-92. DOI
72. Fernández-escamilla, H.; Paez-ornelas, J.; Gutiérrez-lazos, C.; Solís-pomar, F.; Guerrero-sánchez, J.; Pérez-tijerina, E. Bismuth and oxygen vacancies induce (2 × 1) reconstructions in bismuth oxyhalide (BiOX, X = Cl, Br, I) (0 0 1) surfaces. *Appl. Surf. Sci.* **2023**, *618*, 156583. DOI
73. Latthiwan, P.; Hussain, T.; Thongnum, A.; et al. Unveiling polaronic effects on carrier transport in BiOBr, BiOI, and BiOBr-BiOI heterostructures. *ACS. Appl. Energy. Mater.* **2025**, *8*, 8488-99. DOI
74. Li, B.; Liu, X. J.; Zhu, H. W.; Guan, H. P.; Guo, R. T. A review on Bi_2WO_6-based materials for photocatalytic CO_2 reduction. *Small* **2024**, *20*, 2406074. DOI
75. Huang, X.; Soomro, R. A.; Shen, H.; Guo, L.; Yang, C.; Wang, D. Bi_2MO_6 (M = Mo, W) aurivillius oxides for efficient photocatalytic N_2-to-NH_3 conversion: a perspective review. *Inorg. Chem. Front.* **2025**, *12*, 1773-97. DOI
76. Wu, K.; Xu, Z.; Xu, K.; Xu, J.; Zhang, C. Bismuth-based compounds platforms: from fundamentals to chemiresistive gas sensor applications. *Coord. Chem. Rev.* **2026**, *548*, 217174. DOI
77. Zeng, Z.; Wang, Y.; Liu, X.; et al. In-situ precipitation enabled Bi/$BiFeO_3$ schottky junction with an electronic tunnel for promoting photocatalytic ammonia synthesis. *Appl. Catal. B. Environ. Energy.* **2025**, *378*, 125596. DOI
78. Zhang, S.; Xu, J.; Lu, C.; et al. Preparation method investigation and structure identification by XRD and Raman techniques for $A_2B_2O_7$ composite oxides. *J. Am. Ceram. Soc.* **2024**, *107*, 3475-96. DOI
79. Gayen, P.; Saha, S.; Ramani, V. Pyrochlores for advanced oxygen electrocatalysis. *Acc. Chem. Res.* **2022**, *55*, 2191-200. DOI
80. Anantharaman, A. P.; Dasari, H. P. Potential of pyrochlore structure materials in solid oxide fuel cell applications. *Ceram. Int.* **2021**, *47*, 4367-88. DOI
81. Sun, M.; Sun, A.; Wu, Q.; Zhu, H.; Liu, X.; Xing, Y. Synergistic engineering of oxygen vacancies and Schottky junctions for enhanced solar-driven nitrogen fixation on hierarchical hollow $Bi_4Ti_3O_{12}$. *J. Mater. Sci. Technol.* **2026**, *255*, 86-95. DOI
82. Li, P.; Wu, R.; Li, P.; et al. $Bi_2Ti_2O_7$ quantum dots for efficient photocatalytic fixation of nitrogen to ammonia: impacts of shallow energy levels. *Adv. Sci.* **2024**, *11*, 2408829. DOI
83. Feng, M.; Qiu, H.; Jiang, H.; Gao, W.; Lin, J.; Liu, X. Accompanying Bi clusters can effectively enhance the photocatalytic H_2O_2 production performance of $Bi_2Sn_2O_7$/g-C_3N_4 S-Scheme heterostructures. *Carbon* **2025**, *238*, 120253. DOI
84. Gao, F.; Li, W.; Duan, W.; Liao, G.; Wang, C. Improved solar-powered water-splitting performance of $Bi_4Ti_3O_{12}$/TiO_2 composite with synergistically interacted heterointerfaces under platinum cocatalysis. *Small* **2025**, *21*, 2503677. DOI
85. Yang, X.; Cui, D.; Liu, Y.; Xiang, Y.; Li, F. Construction of dual electron channels and multiple active sites in Co-In/Bi/BiOBr for enhanced photocatalytic ammonia production. *J. Colloid. Interface. Sci.* **2025**, *695*, 137806. DOI
86. Sun, A.; Sun, M.; Zhang, R.; Zhu, H.; Xing, Y. Surface and interface engineering of CAU-17/MXene Schottky heterojunction for efficient photocatalytic nitrogen fixation. *Sep. Purif. Technol.* **2025**, *362*, 131939. DOI
87. Xiang, L.; Liu, S.; Zhao, L.; Yuan, S.; Li, X.; Li, N. Modifying the electronic structure of MoS2 via interface engineering to boost intrinsic activity for nitrogen fixation. *J. Alloys. Compd.* **2023**, *945*, 169201. DOI
88. Ranjith, K. S.; Maleki, R.; Ghoreishian, S. M.; et al. Defective phase engineering of S-scheme TiO_2-SnS/SnS_2 core-shell photocatalytic nanofibers for elevated visible light responsive H_2 generation and nitrogen fixation. *J. Mater. Chem. A.* **2024**, *12*, 33818-33. DOI
89. Zhang, L.; Jiang, M.; Tian, H.; et al. Oxygen and nitrogen vacancies in a BiOBr/g-C_3N_4 heterojunction for sustainable solar ammonia fertilizer synthesis. *ACS. Sustainable. Chem. Eng.* **2024**, *12*, 2028-40. DOI
90. Zhang, S.; Si, Y.; Li, B.; Yang, L.; Dai, W.; Luo, S. Atomic-level and modulated interfaces of photocatalyst heterostructure constructed by external defect-induced strategy: a critical review. *Small* **2020**, *17*, 2004980. DOI
91. Zhang, G.; Yuan, X.; Xie, B.; Meng, Y.; Ni, Z.; Xia, S. S vacancies act as a bridge to promote electron injection from Z-scheme heterojunction to nitrogen molecule for photocatalytic ammonia synthesis. *Chem. Eng. J.* **2022**, *433*, 133670. DOI
92. Wu, D.; Hong, L.; Gu, X.; et al. Spherical micro-heterostructured Bi_2MoO_6/Mo-Bi_2O_3 with interfacial oxygen vacancies enabling efficient photocatalytic NH_3 production from N_2 and H_2O. *Catal. Sci. Technol.* **2025**, *15*, 5480-90. DOI
93. Tian, J.; Li, J.; Guo, Y.; Liu, Z.; Liu, B.; Li, J. Oxygen vacancy mediated bismuth-based photocatalysts. *Adv. Powder. Mater.* **2024**, *3*, 100201. DOI
94. Mao, Y.; Wang, P.; Zhan, S. Shedding light on the role of interfacial chemical bond in heterojunction photocatalysis. *Nano. Res.* **2022**, *15*, 10158-70. DOI
95. Chen, C.; Ji, R.; Xia, X.; et al. Dispersed Bi_2S_3 site in a porphyrin-based metal-organic framework for photocatalytic nitrogen fixation. *Appl. Energy.* **2024**, *357*, 122508. DOI

96. Chen, Q.; Zhang, Z.; Chen, Y.; Yu, J. C.; Liu, C.; Wu, L. Fe S bridged CdS/MIL-68(Fe) heterojunction for biomimetic photocatalytic N_2 fixation. *Appl. Catal. B. Environ. Energy.* **2026**, *380*, 125823. DOI
97. He, Y.; Chen, X.; Wu, Z.; Xue, Q.; Tian, F. In situ fabrication of N-doped $Ti_3C_2T_x$-MXene-modified BiOBr Schottky heterojunction with high photoelectron separation efficiency for enhanced photocatalytic ammonia synthesis. *J. Alloys. Compd.* **2023**, *969*, 172470. DOI
98. Li, J.; Feng, J.; Guo, X.; et al. Defect-band bridge photothermally activates type III heterojunction for CO_2 reduction and typical VOCs oxidation. *Appl. Catal. B. Environ.* **2022**, *309*, 121248. DOI
99. Ali, H.; Masar, M.; Guler, A. C.; Urbanek, M.; Machovsky, M.; Kuritka, I. Heterojunction-based photocatalytic nitrogen fixation: principles and current progress. *Nanoscale. Adv.* **2021**, *3*, 6358-72. DOI
100. Zhao, D.; Yang, Y.; Binas, V.; Shen, S. Interface engineering of Z-scheme heterojunction for photocatalytic water splitting. *Fundam. Res.* **2025**, *5*, 2204-8. DOI
101. Xu, Q.; Zhang, L.; Cheng, B.; Fan, J.; Yu, J. S-scheme heterojunction photocatalyst. *Chem* **2020**, *6*, 1543-59. DOI
102. Li, F.; Zhu, G.; Jiang, J.; et al. A review of updated S-scheme heterojunction photocatalysts. *J. Mater. Sci. Technol.* **2024**, *177*, 142-80. DOI
103. Kavitha, R.; Manjunatha, C.; Yu, J.; Kumar, S. Rational design and interfacial engineering of hierarchical S-scheme heterojunction and their photocatalytic applications. *EnergyChem* **2025**, *7*, 100159. DOI
104. Wang, C.; Zhao, Y.; Cheng, C.; Li, Q.; Guo, C.; Hu, Y. S-scheme heterojunction photocatalysts: mechanism, challenges and opportunities. *Coord. Chem. Rev.* **2024**, *521*, 216177. DOI
105. Zhao, C.; Li, X.; Yue, L.; et al. $Bi_4O_5Br_2$ nanoflower and $CdWO_4$ nanorod heterojunctions for photocatalytic synthesis of ammonia. *ACS. Appl. Nano. Mater.* **2023**, *6*, 15709-20. DOI
106. Chen, B.; Hou, Y.; Li, H.; et al. Self-sacrificed BiOBr template-assisted synthesis of α-Bi_2O_3/Bi_3O_4Br heterojunctions with oxygen vacancies for enhanced photocatalytic nitrogen fixation. *J. Colloid. Interface. Sci.* **2023**, *652*, 1857-66. DOI
107. Lan, M.; Zheng, N.; Dong, X.; et al. Facile construction of a hierarchical Bi@BiOBr-Bi_2MoO_6 ternary heterojunction with abundant oxygen vacancies for excellent photocatalytic nitrogen fixation. *Sustain. Energy. Fuels.* **2021**, *5*, 2927-33. DOI
108. Liu, S.; Ren, G.; Meng, X. BrO_3^- bridge Bi_2O_3/$Bi(OH)_3$ heterojunction with multiple charge transfer channels for efficient photocatalytic nitrogen fixation and CO_2 reduction. *ACS. Sustainable. Chem. Eng.* **2023**, *11*, 15599-608. DOI
109. Yue, L.; Zeng, Z.; Ren, X.; et al. Enhanced photocatalytic N_2 fixation using $KNbO_3$/$Bi_4O_5Br_2$ type II heterojunction. *Front. Chem. Sci. Eng.* **2024**, *18*, 66. DOI
110. Vesali-kermani, E.; Habibi-yangjeh, A.; Diarmand-khalilabad, H.; Ghosh, S. Nitrogen photofixation ability of g-C_3N_4 nanosheets/Bi_2MoO_6 heterojunction photocatalyst under visible-light illumination. *J. Colloid. Interface. Sci.* **2020**, *563*, 81-91. DOI
111. Zhao, C.; Li, X.; Yue, L.; et al. Fabrication of novel $BiPO_4$/$Bi_4O_5Br_2$ heterojunctions for improving photoactivity in N_2 fixation and dye degradation. *Mater. Res. Bull.* **2023**, *167*, 112377. DOI
112. Cao, Y.; He, H.; Chang, J.; et al. Surface ion-exchange induced Bi-rich $Bi_{12}O_{17}Cl_2$/BiOCOOH/Bi_2MoO_6 heterojunction with oxygen vacancies for enhanced photocatalytic nitrogen fixation. *Int. J. Hydrogen. Energy.* **2024**, *85*, 335-45. DOI
113. Tang, D.; Wang, Y.; Jing, X.; Duan, C. Construction of a BiOBr-Vo/MIL-101(Fe)-F microsphere heterostructure for photocatalytic nitrogen fixation. *Dalton. Trans.* **2025**, *54*, 10030-6. DOI
114. Xue, X.; Chen, R.; Yan, C.; et al. Efficient photocatalytic nitrogen fixation under ambient conditions enabled by the heterojunctions of n-type Bi_2MoO_6 and oxygen-vacancy-rich p-type BiOBr. *Nanoscale* **2019**, *11*, 10439-45. DOI
115. Shabbir, A.; Sardar, S.; Mumtaz, A. Mechanistic investigations of emerging type-II, Z-scheme and S-scheme heterojunctions for photocatalytic applications - a review. *J. Alloys. Compd.* **2024**, *1003*, 175683. DOI
116. Cao, C.; Huang, Y.; Tian, L.; et al. 2D/2D Bi_2MoO_6/g-C_3N_4 direct Z-scheme Van der Waals heterojunction photocatalyst for boosting nitrogen fixation. *J. Environ. Chem. Eng.* **2025**, *13*, 115019. DOI
117. Wang, H.; Chen, Z.; Shang, Y.; et al. Boosting carrier separation on a BiOBr/$Bi_4O_5Br_2$ direct Z-scheme heterojunction for superior photocatalytic nitrogen fixation. *ACS. Catal.* **2024**, *14*, 5779-87. DOI
118. Chen, L.; Wang, J.; Li, X.; et al. A novel Z-scheme Bi-Bi_2O_3/$KTa_{0.5}Nb_{0.5}O_3$ heterojunction for efficient photocatalytic conversion of N_2 to NH_3. *Inorg. Chem. Front.* **2022**, *9*, 2714-24. DOI
119. Kottarathil, S.; Abhinand, O.; Sridharan, K. In-situ engineered $KBiFe_2O_5$/BiOBr Z-scheme heterojunction photocatalyst for the pharmaceutical pollutant degradation and nitrogen fixation. *Appl. Surf. Sci.* **2026**, *718*, 164869. DOI
120. Cai, J.; Maimaitizi, H.; Okitsu, K.; Tursun, Y.; Abulizi, A. Z-type heterojunction of graphene quantum dots/g-C_3N_4/BiOCl with excellent photocatalytic performance for nitrogen fixation. *Int. J. Energy. Res.* **2022**, *46*, 12147-59. DOI

121. Bai, Y.; Osman, H.; Lin, H.; et al. Synthesis of a novel $Cu_2O/BiFeO_3@Ti_3C_2$ MXene Z-scheme heterojunction for enhanced photocatalytic wastewater treatment and N_2 fixation: mechanistic insights and optimization. *J. Water. Process. Eng.* **2025**, *73*, 107708. DOI
122. Wang, L.; Wu, X.; Zhang, Y.; et al. Enhancement of built-in electric field strength of BiOCl/NMT Z-scheme heterojunctions through photoinitiated defects for optimized photocatalytic performance. *J. Mater. Chem. C.* **2025**, *13*, 17179-88. DOI
123. Yang, X.; Cui, D.; Zhang, T.; Liu, Y.; Li, F. LSPR-enhanced photocatalytic N_2 fixation over Z-scheme POMOF-derived Cu/WO_2 modified C-BiOBr with multiple active sites. *Inorg. Chem. Front.* **2024**, *11*, 8246-57. DOI
124. Zhang, L.; Meng, Y.; Shen, H.; et al. High-efficiency photocatalytic ammonia synthesis by facet orientation-supported heterojunction Cu_2O@BiOCl[100] boosted by double built-in electric fields. *Inorg. Chem.* **2022**, *61*, 6045-55. DOI
125. Xia, S.; Zhang, G.; Gao, Z.; et al. 3D hollow Bi_2O_3@CoAl-LDHs direct Z-scheme heterostructure for visible-light-driven photocatalytic ammonia synthesis. *J. Colloid. Interface. Sci.* **2021**, *604*, 798-809. DOI
126. Wu, D.; Tian, J.; Xing, Y.; Jin, X.; Ni, G. Fabrication of Z-scheme ZnO/Bi_2O_4 heterojunction photocatalyst with superior photocatalytic nitrogen fixation under visible light irradiation. *Solid. State. Sci.* **2021**, *119*, 106709. DOI
127. Ren, X.; Wang, J.; Yuan, S.; et al. Decoration of $CdMoO_4$ micron polyhedron with Pt nanoparticle and their enhanced photocatalytic performance in N_2 fixation and water purification. *Front. Chem. Sci. Eng.* **2023**, *17*, 1949-61. DOI
128. Fu, R.; Kong, Y.; Wang, G.; et al. Promoting the hydrogen spillover via dual active sites synergistically for efficient photo-driven nitrogen fixation. *Appl. Catal. B. Environ. Energy.* **2025**, *362*, 124671. DOI
129. Xue, Y.; Ma, C.; Yang, Q.; et al. Construction of g-C_3N_4 with three coordinated nitrogen (N_3C) vacancies for excellent photocatalytic activities of N_2 fixation and H_2O_2 production. *Chem. Eng. J.* **2023**, *457*, 141146. DOI
130. Hu, T.; Jiang, G.; Yan, Y.; et al. Facile synthesis of Fe single-atom porous photocatalysts via direct metal atomization achieving efficient photocatalytic nitrogen fixation. *J. Mater. Sci. Technol.* **2023**, *167*, 248-57. DOI
131. Zhang, Y.; Guo, L.; Wang, Y.; et al. In-situ anion exchange based Bi_2S_3/OV-Bi_2MoO_6 heterostructure for efficient ammonia production: A synchronized approach to strengthen NRR and OER reactions. *J. Mater. Sci. Technol.* **2022**, *110*, 152-60. DOI
132. Zhang, Y.; Di, J.; Zhu, X.; et al. Chemical bonding interface in $Bi_2Sn_2O_7$/BiOBr S-scheme heterojunction triggering efficient N_2 photofixation. *Appl. Catal. B. Environ.* **2023**, *323*, 122148. DOI
133. Ren, A.; Liu, Z.; Yuan, S.; Zhang, M.; Lu, T. Constructing S-scheme heterojunction $Cs_3Bi_2Br_9$/BiOBr via in-situ partial conversion to boost photocatalytic N_2 fixation. *J. Colloid. Interface. Sci.* **2025**, *678*, 1203-12. DOI
134. Liu, Z.; Luo, H.; Zhang, M.; et al. The construction of $Cs_3Mo_xSb_yBr_9/BiVO_4$ S-scheme heterojunction photocatalyst for efficient photocatalytic N_2 fixation. *Chem. Eng. J.* **2024**, *491*, 151913. DOI
135. Yue, L.; Zhang, J.; Zeng, Z.; et al. In situ fabrication of an S-Scheme $NaNbO_3/Bi_2O_2CO_3$ heterojunction for enhanced performance in photocatalytic nitrogen fixation. *Langmuir* **2023**, *39*, 13267-78. DOI
136. Zhang, Y.; Yu, X.; Gong, Z.; et al. Facile synthesis of g-$C_3N_4/Bi_4O_5Br_2$ S-scheme heterojunction composite with enhanced photocatalytic performance in nitrogen fixation and contaminant degradation. *Appl. Surf. Sci.* **2025**, *700*, 163100. DOI
137. Pournemati, K.; Habibi-yangjeh, A.; Khataee, A. Synergy of homojunction/heterojunction to enforce photocatalytic performance of BiSI/TiO_2 quantum Dots/TiO_{2-x} nanocomposites in NH_3 generation. *Ind. Eng. Chem. Res.* **2024**, *63*, 17168-80. DOI
138. Han, M.; Sun, M.; Jia, X.; et al. Spatially engineered dual s-scheme heterojunctions with significantly enhanced space charge separation for boosting artificial photosynthetic nitrogen fixation. *Adv. Funct. Mater.* **2026**, *36*, e74936. DOI
139. Li, Y.; Kong, X.; Bao, R.; et al. Robust oxygen vacancy surfaces induce chemical bonding interfaces of $Bi_2Sn_2O_7/Bi_2MoO_6$ S-scheme heterojunction with asymmetric adsorption sites for efficient photocatalytic nitrogen fixation. *Chem. Eng. J.* **2026**, *531*, 173870. DOI
140. Zheng, X.; Wang, X.; Feng, L.; et al. In situ fabrication of 2D-2D Bi/BiOBr ohmic heterojunction for enhanced photocatalytic nitrogen fixation. *ACS. Appl. Mater. Interfaces.* **2024**, *16*, 62107-20. DOI